

1 An alternative AUG codon that produces an N-terminally extended form of the
2 influenza A virus NP is a virulence factor for a swine-derived virus.

3

4 Helen M. Wise^{1,2*}, Eleanor Gaunt^{1*}, Jihui Ping³, Barbara Holzer⁴, Seema Jasim¹, Samantha J.
5 Lycett¹, Lita Murphy¹, Alana Livesey², Russell Brown², Nikki Smith¹, Sophie Morgan⁴,
6 Becky Clark⁴, Katerine Kudryavtseva², Philippa M. Beard^{1,4}, Jonathan Nguyen-Van-Tam⁵,
7 Francisco J. Salguero⁶, Elma Tchilian⁴, Bernadette M. Dutia¹, Earl G. Brown³ and Paul
8 Digard¹

9

10 ¹The Roslin Institute, University of Edinburgh, Easter Bush, Midlothian EH25 9RG, UK.

11 ²Division of Virology, Department of Pathology, University of Cambridge, Tennis Court
12 Road, Cambridge CB2 1QP, UK.

13 ³Department of Biochemistry, Microbiology and Immunology, University of Ottawa, Canada.

14 ⁴The Pirbright Institute, Ash Road, Pirbright, Woking, Surrey GU24 0NF, UK.

15 ⁵Division of Epidemiology and Public Health, University of Nottingham School of Medicine,
16 Clinical Sciences Building, City Hospital Campus, Hucknall Road, Nottingham NG5 1PB,
17 UK.

18 ⁶Public Health England, PHE Porton, Manor Farm Road, Porton Down, Salisbury SP4 0JG,
19 UK.

20 *Equal contributions.

21

22 Current addresses:

23 HMW: Clinical biochemistry, Clock Tower building, Western General Hospital, Edinburgh,
24 EH4 2XU, UK

25 JP: Institute of Immunology, College of Veterinary Medicine, Nanjing Agricultural
26 University, China

27 SJ: MRC-University of Glasgow Centre for Virus Research, Glasgow, G61 1QH, UK

28 SM: Respiratory Medicine Unit, NDM Experimental Medicine, University of Oxford, John
29 Radcliffe Hospital, Oxford, OX3 9DU, UK

30

31 Corresponding author: Paul Digard, paul.digard@roslin.ed.ac.uk

32

33

34 **Abstract**

35

36 The 2009 influenza A virus (IAV) pandemic (pdm2009) was caused by a swine H1N1
37 virus with several atypical genetic features. Here, we investigate the origin and significance
38 of an upstream AUG (uAUG) codon in the 5'-untranslated region of the NP gene. Phylogeny
39 indicated that the uAUG codon arose in the classical swine IAV lineage in the mid 20th
40 Century, and has become fixed in the current triple reassortant, variant pdm2009 swine IAV
41 and human pdm2009 lineages. Functionally, it supports leaky ribosomal initiation *in vitro*
42 and *in vivo* to produce two isoforms of NP: canonical, and a longer “eNP”. The uAUG codon
43 had little effect on viral gene expression or replication *in vitro*. However, in both murine and
44 porcine models of IAV infection, removing the uAUG codon gene attenuated pdm2009 virus
45 pathogenicity. Thus, the NP uAUG codon is a virulence factor for swine IAVs with proven
46 zoonotic ability.

47 **Introduction**

48 The 2009 influenza A virus (IAV) pandemic was caused by a swine-origin H1N1
49 (pdm2009) virus that, although highly transmissible, was markedly less pathogenic and
50 caused substantially lower mortality than 20th Century pandemic strains. Notwithstanding
51 marked regional variation in the incidence of severe disease, estimates place the overall
52 human mortality burden from the pandemic phase of pdm2009 at a similar level to disease
53 caused by the preceding seasonal strains (1,2). Initial sequencing of the pdm2009 virus
54 highlighted several features that could potentially explain this unexpectedly mild
55 pathogenicity phenotype (3). These included a PB2 subunit of the viral RNA polymerase
56 with avian-signature motifs at positions 627 and 701, a disrupted PB1-F2 gene,
57 polymorphisms in the NS1 protein that abrogated host cell translational shut-off activity and
58 removed a PDZ-binding domain, as well as a truncated PA-X gene (3-6). A further unusual
59 feature of the pdm2009 genome is the presence of an upstream AUG (uAUG) codon in the 5'
60 untranslated region (UTR) of segment 5 (7). Segment 5 encodes the viral nucleoprotein (NP);
61 a single strand RNA-binding protein that (along with the viral polymerase) encapsidates the
62 single-stranded IAV genomic RNA segments into ribonucleoprotein (RNP) particles and
63 thereby plays an essential role in supporting viral RNA synthesis (8,9). NP also contains
64 nuclear localisation (NLS) and nuclear export signals and, in concert with the viral matrix
65 (M1) and nuclear export protein (NEP) as well as many cellular proteins, helps direct the
66 nuclear import of the viral genome at the start of infection and its export after genome
67 replication (9). This functional importance is reflected in a high level of sequence
68 conservation across IAV strains (10) and unlike the viral HA, NA and NS1 proteins, length
69 polymorphisms of NP are very rare. However, the NP uAUG codon is in frame with the main
70 NP open reading frame (ORF) and, if used for translation initiation, would add an extra 6
71 amino-acids to the N-terminus of the protein. The N-terminal 20 amino acids of NP form a

72 flexible region not visible in crystal structures of the polypeptide (11,12) and contain the
73 primary NLS of the polypeptide responsible for nuclear import of monomeric NP and RNPs
74 (13-15). It was therefore reasonable to hypothesise that an alteration to this region to produce
75 an extended NP (eNP) variant would have functional consequences for the protein that could
76 downregulate viral pathogenicity, thus providing an explanation for the unexpectedly low
77 levels of morbidity seen during the 2009 pandemic. Here, we describe a test of this
78 hypothesis that shows that while eNP is produced in infection and the uAUG codon does
79 affect *in vivo* viral pathogenicity in mice and pigs, it unexpectedly acts to increase virulence.

80

81 **Results**

82

83 **The NP uAUG codon is of swine IAV origin**

84 Segment 5 of the pdm2009 virus was acquired from the H1N1 classical swine virus
85 lineage which in turn is a descendant of the 1918 pandemic strain, which lacked the uAUG
86 (16,17). Examination of all available IAV segment 5 sequences on the Genbank database that

87

88 **Table 1.** Prevalence of the uAUG in IAV segment 5 sequences

89

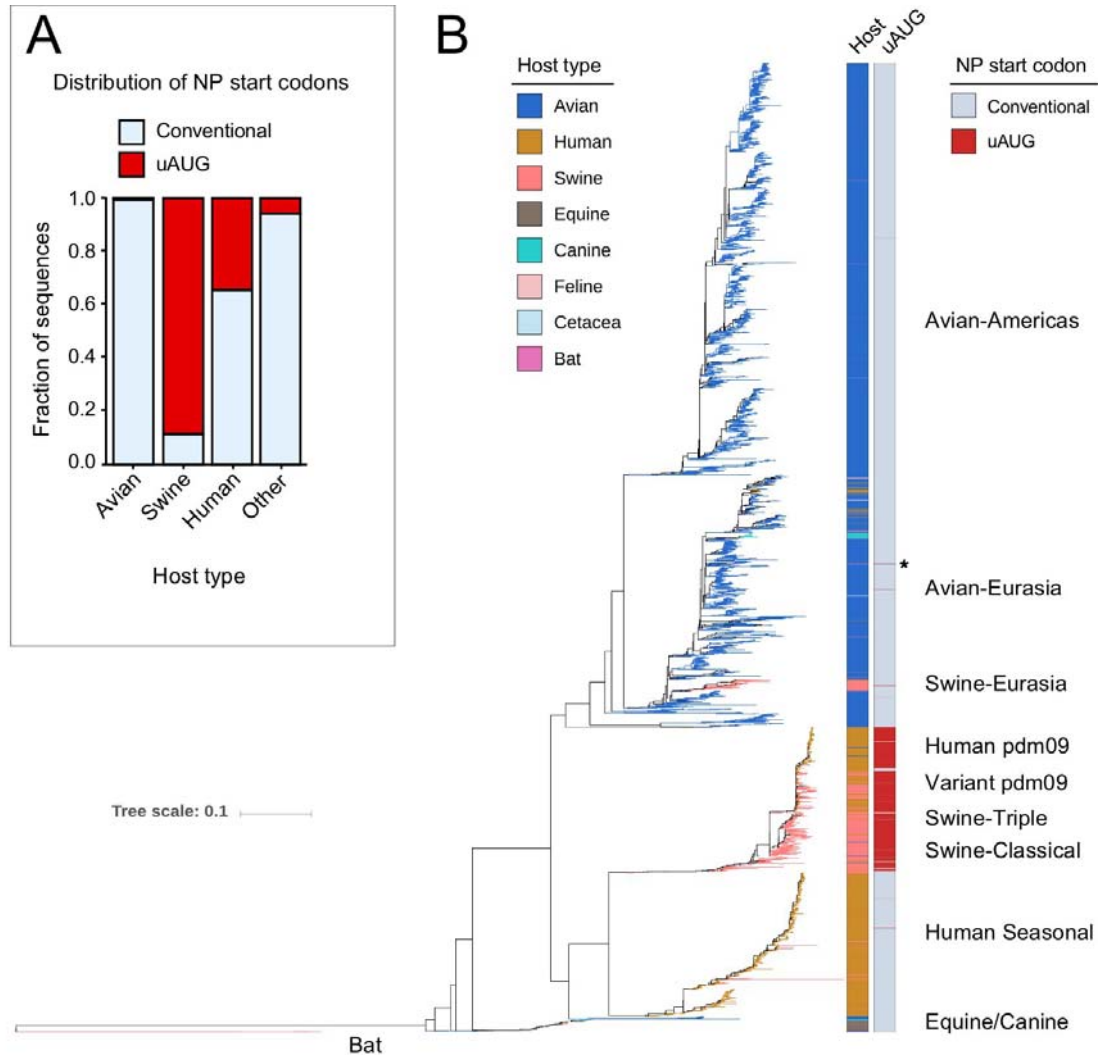
Host	Number of sequences	Conventional Start	uAUG start (%)
Avian	11210	11176	34 (0.3)
Swine	2396	261	2135 (89.1)
Human	19772	12852	6920 (35.0)
Other	244	229	15 (6.1)
Total	33622	24518	9104 (27.1)

90

91 reported the 5'-UTR indicated that possession of the uAUG is a minority trait, with 9104 of
92 33622 sequenced viruses (27%) containing it. However, within this overall population, there
93 were clear differences between viruses from different host species (Fig 1A, Table 1), with the
94 uAUG being extremely rare in avian isolates (~ 0.3%) but very frequent (approaching 90%)

95 in swine viruses. Around one third of human isolates contain the segment 5 uAUG, with the
96 vast majority of these being pdm2009 isolates.

97



98

99 **Figure 1.** Phylogenetic analysis of segment 5 uAUG occurrence. (A) The fraction of segment 5 sequences that
100 report the 5'-UTR, split into broad host categories, that contain the uAUG codon (red) or only the
101 conventional NP start codon (blue). (B) Maximum likelihood phylogenetic tree of stratified subsampled
102 sequences. Tips and left hand bar are coloured according to host while the right hand bar reports the
103 presence (red) or absence (blue) of the uAUG start codon. Major lineages are indicated. The section of
104 the tree indicated with an asterisk is reported in greater detail in Figure S4.

105

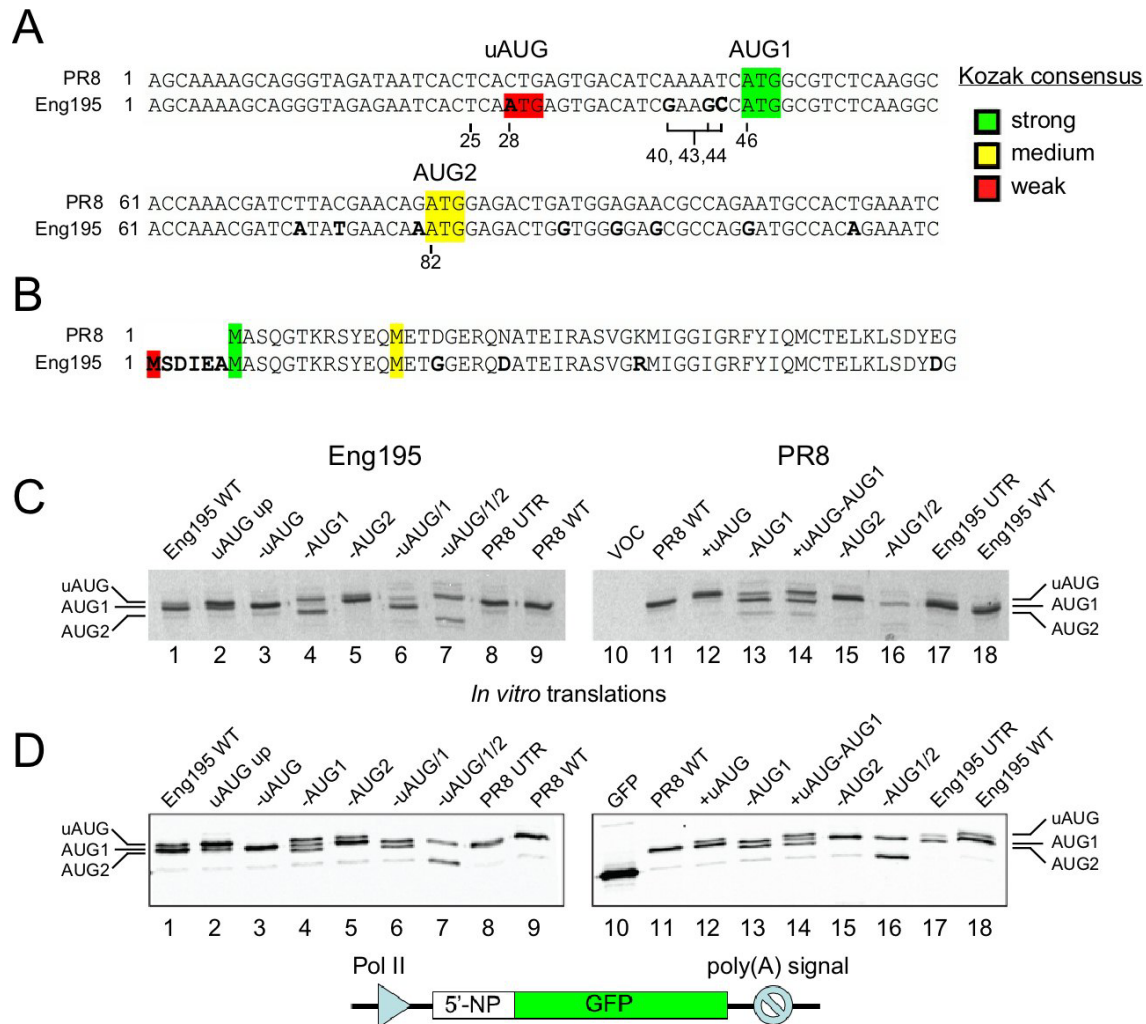
106 To examine the evolution of the uAUG in IAV, a phylogenetic tree for segment 5 was
107 constructed from a stratified subsampled dataset of over 6000 sequences (Tables S1, S2) and
108 coloured according to host species and the presence or absence of the uAUG (Fig 1B). This
109 indicated that the uAUG is primarily a feature of the classical swine virus segment 5 and, by
110 descent (18), the triple reassortant, pdm2009 and variant pandemic lineages (Table S1, Table
111 S2, Fig S1). Within this clade, the uAUG codon evolved in the early 1960s in the US swine
112 population, becoming predominant by the 1970s (Fig S2). The uAUG polymorphism also
113 shows almost complete fixation in the subsequent triple reassortant, pdm2009 and variant
114 swine virus lineages (93% of the sequences analysed; Fig S3, Table S1). In addition, the
115 uAUG appears to have arisen independently on several other occasions: two or three times
116 each in the avian and human seasonal H3N2 lineages, detectably persisting for no more than
117 two or three years at most (Table S3), as well as twice within swine IAVs. One of the swine
118 episodes reflects a relatively short-lived occurrence, in which an H5N1 virus transferred from
119 ducks to pigs (19), gaining the uAUG codon around the time of the epizootic transition (Fig
120 S4). The other occasion represents a localized gain of the uAUG within the Eurasian swine
121 IAV lineage in Hong Kong in the early/mid 2000s (Fig S5). Thus overall, segment 5 has
122 gained the uAUG codon on at least seven occasions; three of these were associated with
123 swine IAV and the first of these, acquired in the background of a segment from the 1918
124 pandemic virus, has persisted for over half a century and resulted in world-wide colonization
125 of swine, and via the 2009 pandemic, man.

126

127 **Initiation of translation occurs from the segment 5 uAUG in cell-free and cell-based** 128 **systems**

129 The phylogenetic data suggested the hypothesis that the uAUG provided a host-
130 specific selective advantage in H1N1 viruses. As a first test of its biological significance, we

131 asked if it was used for translation. The uAUG arises from a C28A polymorphism and is in
 132 frame with the canonical start codon of the NP ORF (AUG1) such that, if used, it would



133

134 **Figure 2.** Sequence and translation initiation potential of IAV segment 5. (A) Nucleotide sequence of
 135 the 5'-end (mRNA sense, starting from position 1 of cRNA; *i.e.* ignoring any cap-snatched leader sequence) of
 136 segment 5 from PR8 and Eng195 strains. Differences are highlighted in bold, while AUG codons are colour-
 137 coded according to their Kozak initiation potential. Numbered positions were targeted for mutagenesis. (B)
 138 Amino-acid sequence of the N-terminal region of NP, highlighted as above. (C) Aliquots of rabbit reticulocyte
 139 lysate coupled *in vitro* transcription/translation reactions supplemented with ³⁵S-methionine were programmed
 140 with pDUAL plasmids containing cDNA copies of the indicated WT and mutant segment 5s (or empty vector;
 141 VOC) before separation by SDS-PAGE. Radiolabelled translation products were detected by autoradiography.
 142 (D) Lysates from 293T cells transfected with plasmids containing the 5'-201 nucleotides of segment 5 cDNA,
 143 either WT or mutated as labelled, fused in frame with GFP (or with a plasmid only encoding GFP) were
 144 separated by SDS-PAGE and western blotted for NP. The migration position of polypeptides starting at the first
 145 three AUG codons is indicated.

146 produce an extended NP polypeptide with a 6 amino-acid extension (Figs 2A, B). However,
147 the uAUG codon is in a poor 'Kozak' context for translation initiation (20) so it was unclear
148 if, or to what extent, it might be seen by scanning ribosomes and used for translation
149 initiation. A similarly poor context AUG codon near the 5'-end of segment 2 of IAV is not
150 seen by scanning ribosomes to any appreciable extent (21). To address whether the segment 5
151 uAUG is used for translation, we created a series of constructs based on segment 5 cDNA,
152 from either the UK prototype pdm2009 virus A/England/195/2009 (Eng195) (22) or the
153 laboratory-adapted A/Puerto Rico/8/34 (PR8) H1N1 strain, with mutations designed to alter
154 potential translation start sites in the first 100 nucleotides. These included removing the
155 uAUG from Eng195 or adding it to PR8 by A28C/C28A switches, altering AUGs 1 and 2 to
156 CUG codons, improving the Kozak consensus sequence of uAUG (by U25G) and
157 reciprocally swapping the context of AUG1 (by mutating nucleotides 40, 43 and 44) between
158 Eng195 and PR8 identities (Fig 2A).

159 These plasmids were then used to programme radiolabelled coupled *in vitro*
160 transcription-translation reactions in rabbit reticulocyte lysate and polypeptide synthesis was
161 monitored by SDS-PAGE (run for longer than normal to separate polypeptides predicted to
162 differ in molecular weight by < 1 kDa) and autoradiography. The wild type (WT) PR8
163 plasmid directed synthesis of a single major polypeptide species whereas WT Eng195 gave a
164 doublet in which the slower migrating species was less abundant (Fig 2C, compare lane 1
165 with 9, and lane 11 with 18), consistent with translation initiation at either of two closely
166 spaced AUG codons in the Eng195 segment 5 mRNA. Further supporting this conclusion,
167 improving the Kozak consensus of the Eng195 uAUG altered the proportions of the doublet
168 so that the upper band was predominant, while mutating the uAUG removed it (Fig 2C, lanes
169 2 and 3). Confirming the likely identity of the polypeptides, mutation of AUG1 to CUG
170 further changed the ratio of the doublet species, with only a trace of the smaller polypeptide

171 now visible, but with the addition of a more prominent faster migrating band (lane 4) that co-
172 migrated with trace species visible in WT and other AUG1-containing translation reactions.
173 Mutation of AUG2 removed this fast-migrating product (lane 5), suggesting that leaky
174 ribosomal scanning past an inefficiently recognised uAUG in the absence of AUG1 led to
175 increased usage of AUG2 for translation initiation. The small amount of a polypeptide with
176 the expected size for canonical NP seen when AUG1 was replaced with CUG most likely
177 arose from non-AUG initiation at a CUG codon in a strong Kozak consensus (23,24), as the
178 alternative mutation of AUG -> AGG blocked its formation (data not shown). Pairwise
179 knockouts of the first three AUG codons in Eng/195 segment 5 also indicated leaky
180 ribosomal scanning leading to context-dependent recognition of all three start sites (lanes 6
181 and 7). Creation of the equivalent mutations in the PR8 NP gene showed that similar rules
182 applied; addition of uAUG led to production of a closely spaced NP doublet (Fig 2C,
183 compare lanes 11 and 12), while mutating combinations of uAUG, AUG1 and AUG2 showed
184 that the hierarchy of translation initiation potential *in vitro* was AUG1 > uAUG >> AUG2
185 (lanes 13-16). However, swapping the entire 5'-UTRs of Eng/195 and PR8 had little effect
186 beyond that of the addition or omission of the uAUG (compare lanes 8 and 9, 17 and 18),
187 suggesting that the nucleotide polymorphisms at positions 40, 43 and 44 were of little
188 significance for initiation at AUG1.

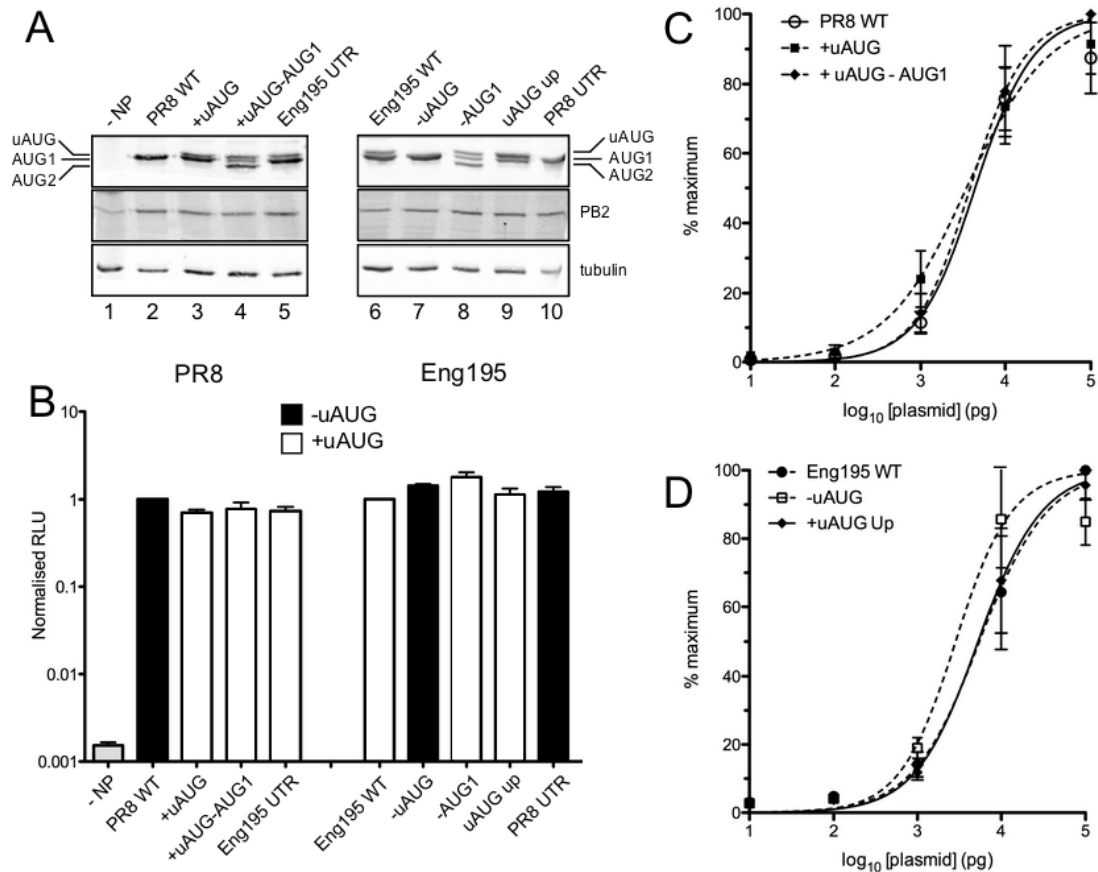
189 The coupled *in vitro* transcription-translation system we used did not generate
190 mRNAs with 5'-cap structures and nor was it optimised for KCl concentration, leading to the
191 possibility of less accurate translation initiation than would occur in intact cells (25). We
192 therefore tested NP expression after transfection of 293T cells with a corresponding set of
193 plasmid constructs containing the first 201 nucleotides of segment 5 cDNA fused in frame to
194 the green fluorescent protein (GFP) ORF (Fig 2D). This cloning strategy kept the 5'-end of
195 the viral sequences intact but decreased the overall size of the expected polypeptides from ~

196 56 kDa to ~ 34 kDa, thus aiding separation of the various isoforms, as well as permitting their
197 detection by western blotting for GFP. In this system, all plasmids with an IAV UTR
198 produced a low abundance product with the same mobility as GFP (compare lanes 10 and
199 11). However, in addition to this, a construct with the WT PR8 UTR produced a single major
200 species while the WT Eng195 plasmid produced a clearly separated doublet (Fig 2D,
201 compare lanes 1 and 8, and lanes 11 and 18). As before, the relative abundance of the Eng195
202 upper doublet species was increased by a mutation that improved the Kozak consensus of the
203 uAUG while its synthesis was blocked by removal of the uAUG (lanes 2 and 3). Again,
204 similarly to the outcome of the *in vitro* translation experiments, mutation of AUG1 to CUG
205 produced a triplet species whose upper and lower constituents could be explained by
206 initiation at the uAUG and AUG2 in the absence of AUG1, as well as lower levels of CUG
207 codon-directed translation initiation at the mutated AUG1 codon (compare lane 4 with lanes
208 5-7). Analysis of the counterpart mutations in a PR8 background produced corresponding
209 results; introduction of the uAUG gave a doublet NP species (lane 12) while AUG2 was only
210 used for translation initiation after mutation of AUG1 to CUG had downregulated but not
211 abolished initiation at the canonical NP start site (lanes 13-16). Thus, the NP uAUG codon
212 was seen by scanning ribosomes in a cellular context as well as *in vitro* to produce eNP,
213 although AUG1 remained the preferred start site. In contrast to the cell-free setting,
214 translation initiation at AUG2 could only be detected in the absence of AUG1.

215

216 **eNP is functionally equivalent to canonical NP in supporting viral gene expression and**
217 **replication in cells**

218 Next, we examined the effect of a subset of these mutations on the ability of NP to
219 support viral gene expression, using an assay in which RNPs were reconstituted by
220 transfection of cells with plasmids encoding the three subunits of the viral RNA



221

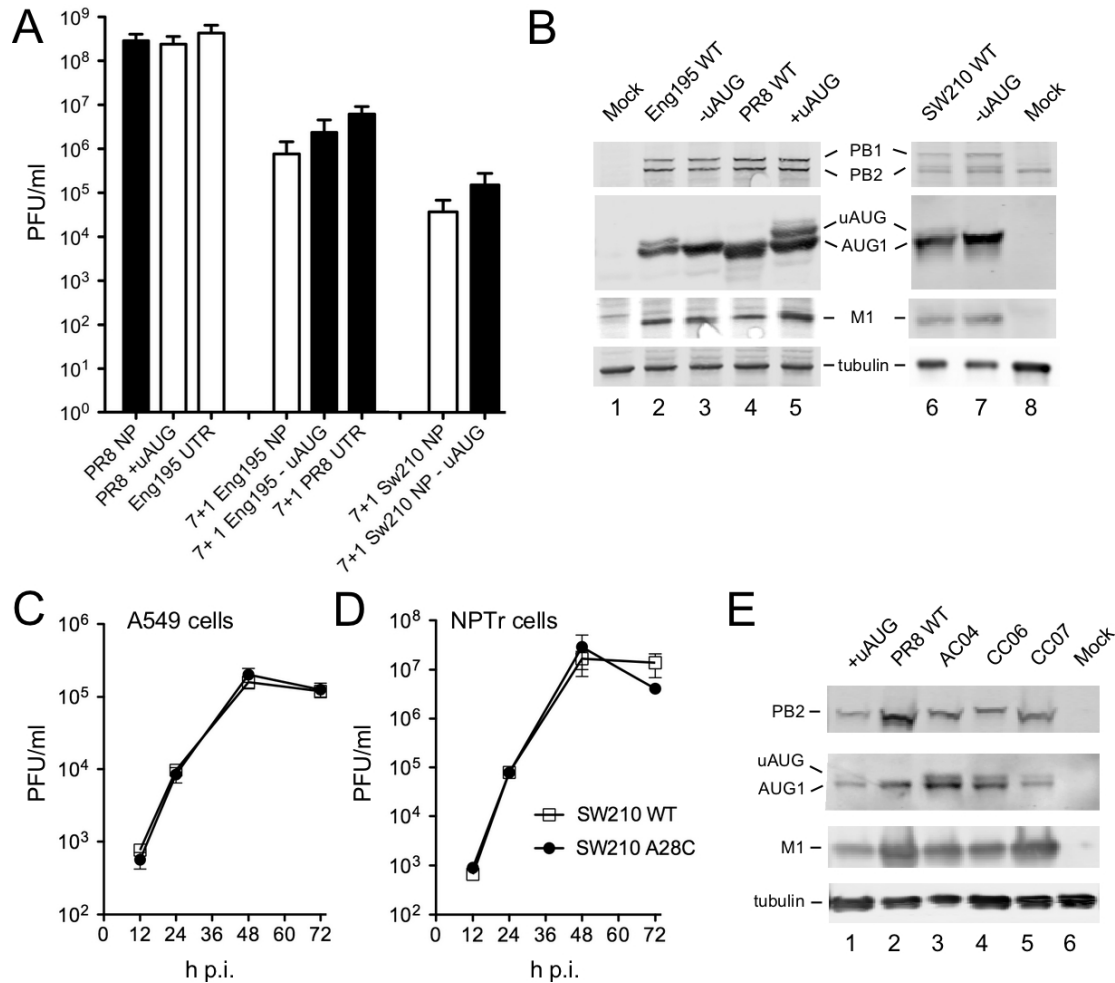
222 **Figure 3.** Ability of NP mutants to support viral gene expression in RNP reconstitution assays. 293T cells were
 223 transfected with reverse genetics plasmids encoding the 3 polymerase proteins (from PR8 or Eng195 as
 224 indicated), WT or mutant forms of NP and a vRNA-like reporter segment encoding luciferase, thus
 225 reconstituting RNPs. (A) Cell lysates were analysed by SDS-PAGE and western blotting for the
 226 indicated polypeptides. (B) Luciferase activity in the lysates was measured and normalised to the
 227 amount seen with the corresponding WT gene. Data are the mean \pm SEM of four independent
 228 experiments. Differences between samples with a complete RNP were non-significant (repeated
 229 measures ANOVA with Dunnett's multiple comparison test comparing against the matched WT) (C, D)
 230 Luciferase activity was measured from RNP reconstitution assays in which the NP plasmid was titrated
 231 and all other plasmids kept constant and normalised to the maximum activity within an individual
 232 titration set. Data are the mean \pm SEM of 3-6 independent experiments, curve fitted to a variable slope
 233 log₁₀ [agonist]-response model using Graphpad Prism. The 95% confidence limits of the estimated EC₅₀
 234 values within groups overlapped, indicating non-significance (data not shown).

235

236 polymerase (3P) and WT or mutant copies of the NP gene (26,27), along with a vRNA-like
 237 reporter segment with an antisense luciferase gene. First, NP expression was examined by

238 western blotting, where again, the presence of an uAUG codon in both PR8 and Eng195
239 backgrounds led to production of an NP doublet whose relative abundance varied according
240 to the strength of the uAUG Kozak consensus (Fig 3A). Reconstitution of both WT PR8 and
241 Eng195 RNPs led to around 300-fold increases in luciferase expression compared to a control
242 reaction lacking NP (Fig 3B). However, at a fixed dose of NP plasmid, all of the mutants had
243 comparable activity to their WT counterpart, with no more than 2-fold differences evident.
244 To provide a more sensitive examination of NP activity, we titrated the amounts of NP
245 plasmid and fitted the luciferase expression values to a variable slope dose-response enzyme
246 kinetic model. The resulting curves for both the PR8 and Eng195 sets of plasmids were very
247 similar (Fig 3C, D) and the estimated concentrations of plasmid required for half-maximal
248 activity were not significantly different. Thus, the precise identity of the N-terminus of NP
249 had little influence on viral gene expression, even at limiting amounts of the protein.

250 We then examined what effect the presence of the uAUG codon had on virus
251 replication *in vitro*. End-point titres following low multiplicity infection of MDCK cells with
252 WT PR8 or variants with the uAUG codon added to PR8 segment 5 were essentially the same
253 (Fig 4A, left hand bars). When the counterpart experiment was performed for viruses with
254 segment 5 from either Eng195 or another early isolate from the 2009 pandemic,
255 A/Halifax/210/2009 [SW210; (28)] (both as 7:1 reassortants on the PR8 background to
256 confer efficient infection of MDCK cells), removal of the uAUG codon with an A28C
257 mutation gave slight increases (4-5 fold) in average titres while replacing the normal Eng195
258 UTR with the PR8 sequence gave an 8-fold increase (Fig 4A, middle and right hand bars).
259 However, none of these differences were statistically significant. Western blot analysis of
260 lysates from cells infected at high multiplicity confirmed that the A28C polymorphism
261 behaved as expected with respect to production or not of the two NP isoforms



262

263 **Figure 4.** Expression and functional significance of eNP for virus replication *in vitro*. (A) MDCK cells were
 264 infected at an MOI of 0.01 with the indicated viruses and titres measured at 48 h p.i.. Data are the mean
 265 ± SEM of 4-5 independent experiments. Differences within groups were not statistically significant
 266 (PR8, Eng195; One way ANOVA with Tukey's post test, Sw210; *t*-test). (B) Cell lysates from A549
 267 cells infected at an MOI of 5 and harvested at 24 h p.i. were analysed by SDS-PAGE and western
 268 blotting for the indicated polypeptides (uAUG/AUG1 = NP). (C, D) A549 or NPTr cells were infected
 269 an an MOI of 0.03 and samples titred at the indicated times p.i. Data are the mean ± SEM of three
 270 independent experiments. (E) Lysates from MDCK-SIAT cells infected with the indicated viruses at
 271 high MOI and harvested at 16 h p.i. were analysed by SDS-PAGE and western blotting for the
 272 indicated polypeptides.

273

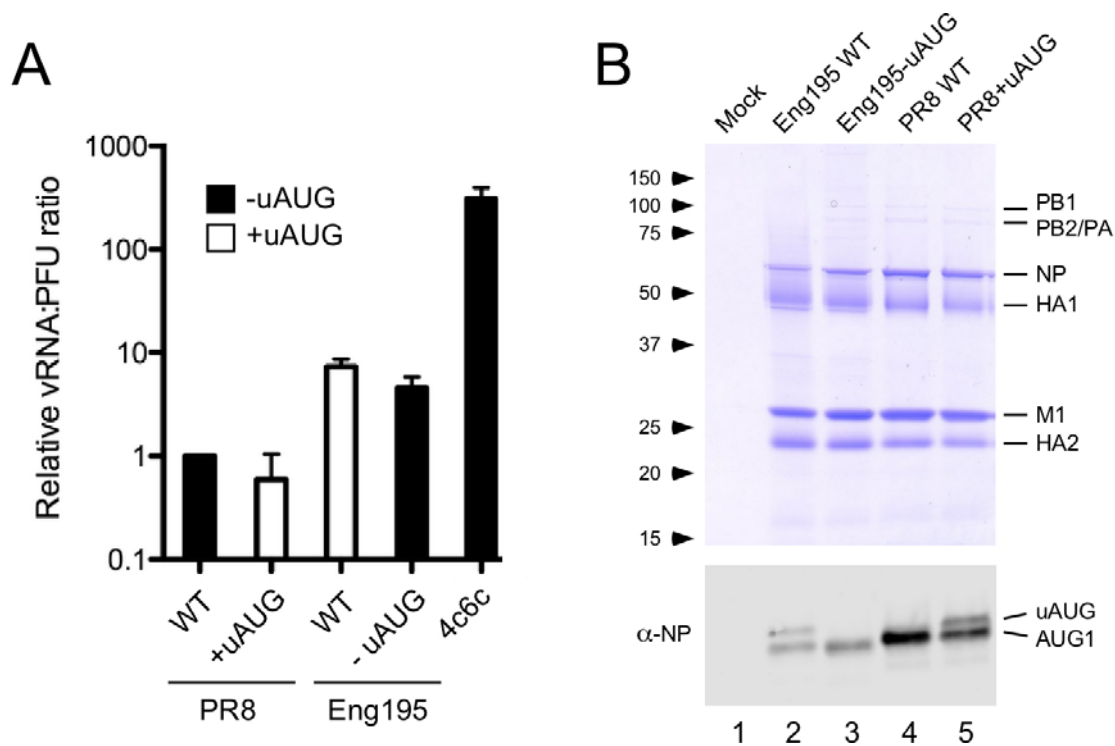
274 in all virus backgrounds, without affecting synthesis of other viral structural proteins (Fig
 275 4B). Since our clone of the Eng195 virus does not infect or replicate well in the continuous

276 cell lines commonly used to study IAV replication, we tested the full SW210 virus under
277 multicycle growth conditions in human A549 cells or swine new-born pig tracheal (NPTr)
278 cells. WT and A28C mutant viruses replicated with almost identical kinetics in both cell
279 types (Figs 4C, D). Thus the presence or absence of the segment 5 uAUG codon and
280 expression of eNP had little effect on IAV replication *in vitro*.

281 Given the high proportion (97.9%) of pdm2009 isolates encoding uAUG (Table S1),
282 we analysed three clinical isolates with known, limited *in vitro* passage histories (29) by
283 western blotting following high multiplicity infection of MDCK-SIAT cells. All three viruses
284 produced both NP and eNP (Fig 4E), further supporting the potential *in vivo* relevance of
285 eNP expression.

286 The terminal regions of IAV genome segments are involved in vRNA packaging, via
287 specific RNA signals (30). To test whether the mutations that added or subtracted the uAUG
288 codon affected segment 5 packaging, RNA was extracted from independently grown stocks
289 of WT or mutant viruses and the amount of segment 5 measured by qRT-PCR. The values
290 obtained were then considered as a ratio to the plaque titre of the stocks, normalised to WT
291 PR8, to produce a relative vRNA:PFU ratio. As a positive control for a virus with a
292 packaging defect, we analysed a PR8 mutant with two clusters of synonymous mutations (9
293 nucleotide changes in total) introduced into the 5'-ends of segments 4 and 6, where
294 bioinformatics analyses had predicted the likely location of packaging signals (31). The
295 genome copy:PFU ratio of this “4c6c” virus was elevated by over 2 log₁₀ compared to WT
296 virus (Fig 5A). In contrast, introduction of the C28A mutation into PR8 had very little effect

297 on the quantity of segment 5 required to form an infectious unit. Replacement of PR8



298

299 **Figure 5.** Virion composition of PR8 and PR8 7:1 reassortants containing the Eng195 segment 5 (Eng195). (A)
300 The segment 5 vRNA content of virus stocks of known infectious titre was determined by qRT-PCR and the
301 values used to derive genome:PFU ratios, normalised to that of WT PR8. Data are the mean \pm range of two
302 independent replicates. (B) Aliquots of sucrose gradient purified virus or the corresponding fraction from
303 uninfected allantoic fluid was analysed by SDS-PAGE and (upper panel) Coomassie Blue staining or (lower
304 panel) western blotting for NP. The migration positions of molecular mass standards (kDa) and major viral
305 structural proteins are indicated. Note that the gel used for the lower panel was run further to separate the two
306 NP isoforms.

307

308 segment 5 with the corresponding WT Eng195 vRNA elevated the genome:PFU ratio by ~
309 10-fold, suggestive of a packaging incompatibility between the PR8 backbone and the
310 pdm2009 segment. However, addition of the A28C mutation into the Eng195 segment to
311 remove the uAUG codon did not worsen this phenotype. Overall therefore, the data did not
312 indicate any large effect of the A28C polymorphism on segment packaging.

313

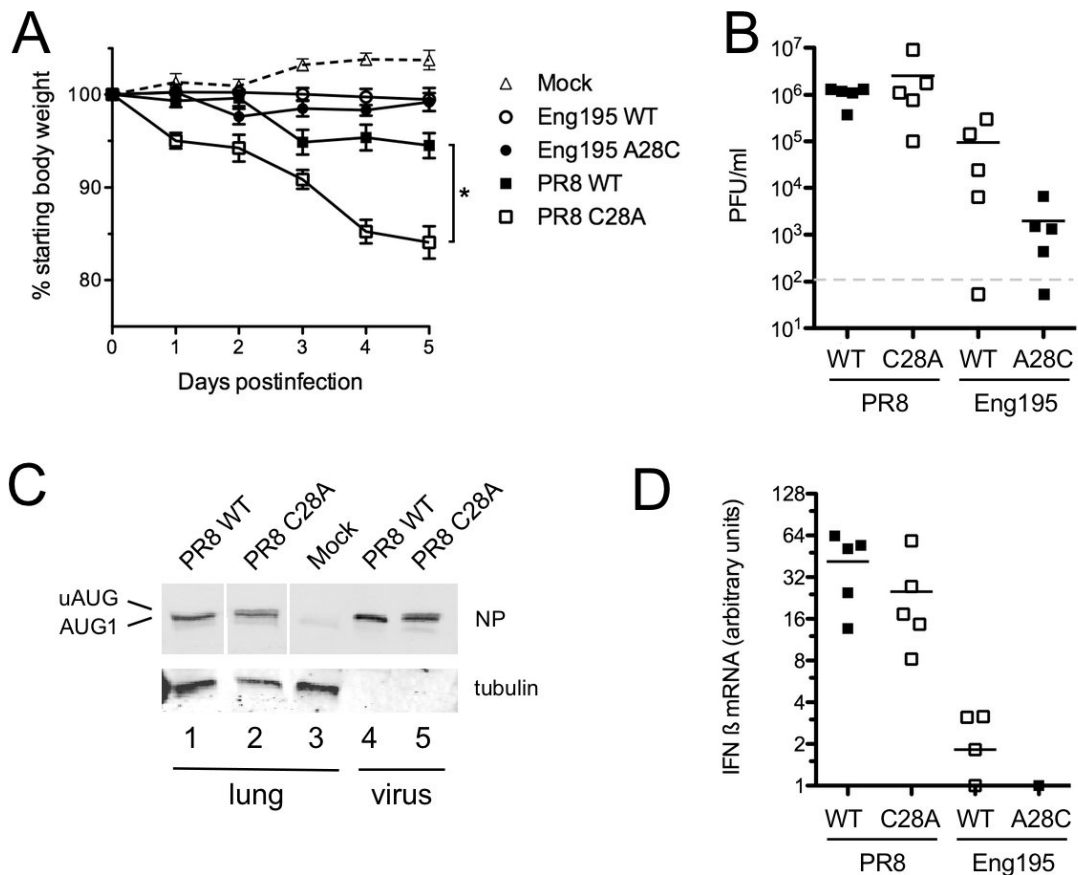
314

To determine if eNP is incorporated into virus particles, virus stocks were grown in embryonated hens' eggs and virions purified from allantoic fluid by pelleting through a

315 sucrose cushion followed by banding on a sucrose velocity gradient. SDS-PAGE and
316 Coomassie blue staining of the resulting material showed the presence of the expected major
317 viral structural proteins (Fig 5B, top panel). Re-analysis of the same material by western
318 blotting for NP under PAGE conditions sufficient to separate the two forms of NP clearly
319 showed the presence of both canonical and eNP in an approximately 2:1 ratio in viruses
320 where the uAUG codon was present (Fig 5B, bottom panel). Thus consistent with its
321 apparently normal function in minireplicon assays, eNP was incorporated into virus particles.
322

323 **The C28A polymorphism influences pathogenesis in mice**

324 To examine the role of eNP *in vivo*, the mouse model of IAV infection was used.
325 First, groups of BALB/c mice were infected with PR8 or the PR8:Eng195 segment 5
326 reassortant in either WT form or with the C28A polymorphism, and weight loss followed
327 over 5 days. Uninfected mice gained weight over time, while mice infected with WT PR8 lost
328 around 5% of their starting body weight (Fig 6A). Unexpectedly, the PR8 C28A mutant
329 induced significantly greater weight loss in the animals, resulting in an average loss of over
330 15%. Consistent with this, the PR8 C28A-infected mice showed increased clinical signs
331 compared to their WT-infected counterparts, including increased respiratory rate, lower
332 motility, more extreme staring of the coat and more emphatic hunching (data not shown).
333 Animals infected with the PR8:Eng195 segment 5 WT or A28C viruses did not show obvious
334 clinical signs or lose any substantial amount of weight over the 5 days (Fig 6A). At day 5, all
335 animals were sacrificed and the lungs collected for further analyses. When viral loads were
336 measured, both WT and C28A PR8 viruses gave titres of around 10^6 PFU/ml of homogenate
337 (Fig 6B). The reassortant virus with WT Eng195 segment 5 produced titres of around 10^5



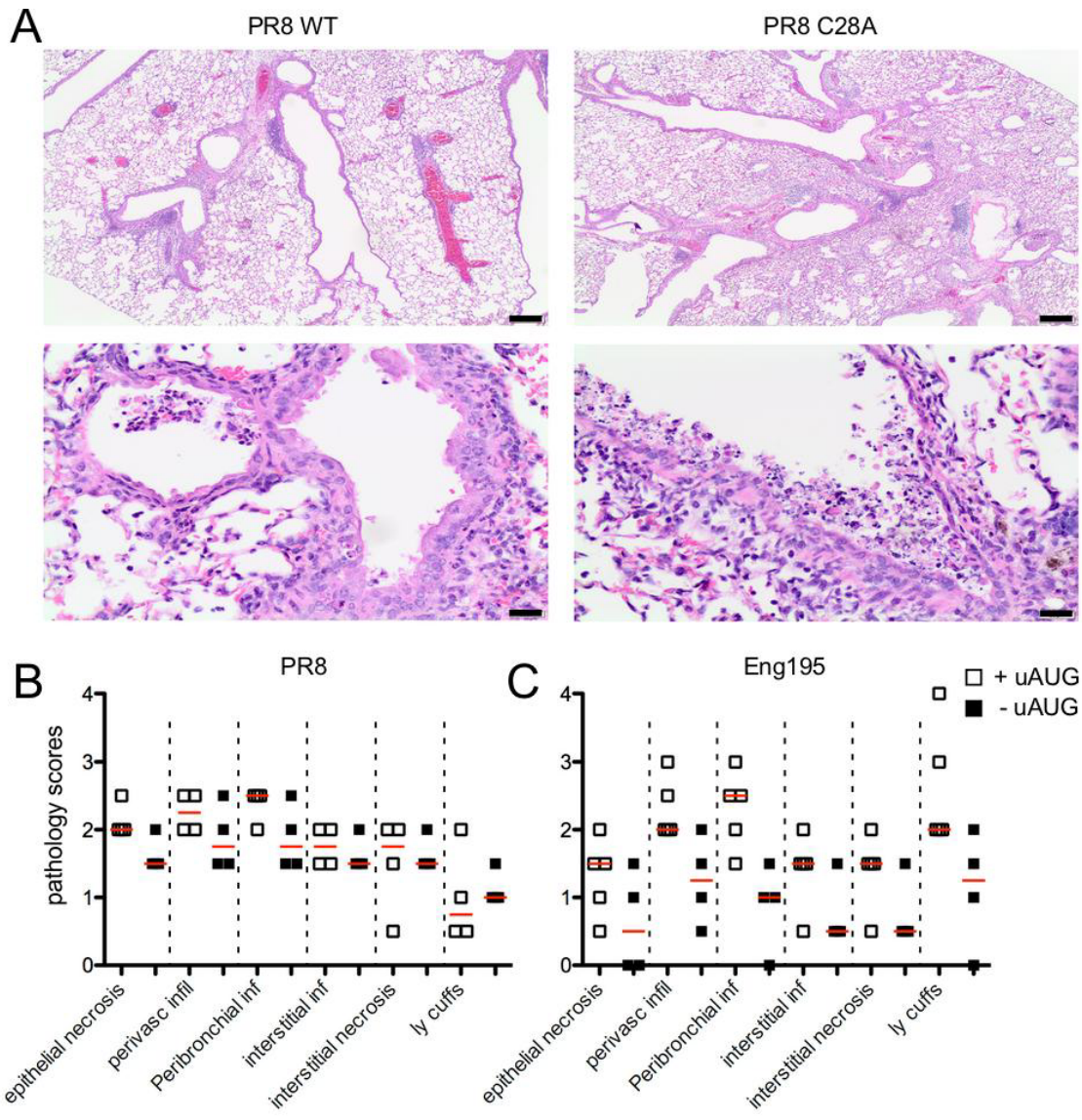
338
339

340 **Figure 6.** Pathogenesis of eNP-expressing viruses in Balb/c mice. Groups of 5 six-week old mice were infected
 341 with 200 PFU or PR8 viruses or 500 PFU of 7:1 PR8 reassortant viruses containing the Eng195 segment
 342 5 (Eng195). (A) Body weight was measured daily for 5 days after infection. Data are plotted as the
 343 mean \pm SEM. * $p < 0.05$ (One way ANOVA with Tukey's multiple comparison post test; WT PR8
 344 versus PR8 C28A). (B) Animals were euthanised at day 5, the left lungs homogenised and virus titres
 345 determined. Dashed line indicates limit of detection. Differences between pairs of viruses were non-
 346 significant, as assessed by *t*-tests. (C) Aliquots of pooled lung homogenate (lung) or purified virus
 347 (virus) were analysed by SDS-PAGE and western blotting for the indicated proteins. (D) RNA was
 348 extracted from the left lung tip and IFN β and GAPDH mRNA levels determined by qRT-PCR. IFN β
 349 transcript was not detected in RNA from uninfected animals, so positive values were corrected for
 350 GAPDH levels and then expressed relative to the lowest samples that gave a C_t value (one animal each
 351 from WT and A28C Eng195 infections). Differences between virus pairs were not statistically
 352 significant (non-parametric *t*-tests).

353 PFU/ml, despite the lack of clinical signs of infection. However, the corresponding A28C
 354 mutant lacking the uAUG codon gave substantially lower (on average, almost 2 \log_{10}) titres,
 355 suggesting attenuated virus replication. Examination of lung homogenates by western

356 blotting for viral NP confirmed that the PR8 C28A virus expressed eNP *in vivo* (Fig 6C).
357 Neither form of NP could be detected in material from animals infected with the PR8:Eng195
358 reassortant viruses, most likely because of the lower levels of virus replication. To measure
359 innate immune response stimulation, levels of IFN- β mRNA in the lung homogenates were
360 assessed by qRT-PCR. Transcripts were undetectable from mock infected mouse lung but
361 were clearly induced by PR8 virus infection (Fig 6D). However, despite the more severe
362 disease seen with the PR8 C28A virus, there was no significant difference between this and
363 WT virus samples. IFN- β mRNA levels were substantially lower in animals infected with the
364 WT PR8:Eng195 virus and were undetectable in all but one animal infected with the A28C
365 mutant (Fig 6D); these differences plausibly correlated with virus load (Fig 6B). A similar
366 outcome was obtained when a broader array of cytokines and chemokines were analysed; few
367 differences of note between the PR8 pair of viruses and generally higher induction from WT
368 Eng195 than its A28C counterpart (Fig S6).

369 To assess histopathological changes in the mice, formalin-fixed lung sections were
370 stained with haematoxylin and eosin and examined by a veterinary pathologist. Changes
371 identified in infected mice were consistent with acute to subacute IAV infection; these were
372 characterised by degeneration and necrosis of epithelial cells lining airways, accompanied by
373 peribronchial and perivascular inflammation, as well as interstitial inflammation and necrosis
374 (Fig 7A and data not shown). The inflammatory infiltrate consisted of lymphocytes and
375 macrophages with fewer plasma cells, and rare neutrophils and eosinophils. When the slides
376 were scored blind for various pathological features, the C28A PR8 mutant gave generally
377 higher scores than WT PR8 in most categories (Fig 7B). Combining these scores along with a
378 consideration of the area of lung affected by pathological changes to give an overall score
379 showed significantly higher ($p < 0.05$, *t*-test) damage from the PR8 C28A virus (Table S4).



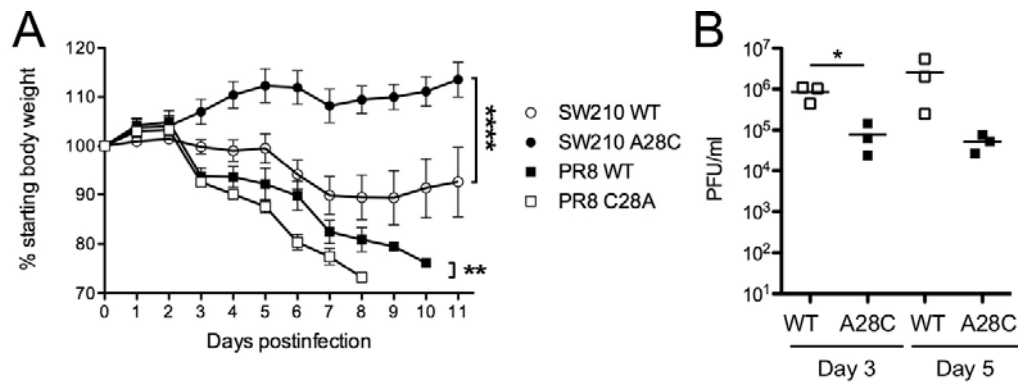
380

381 **Figure 7.** Histopathology of eNP-expressing viruses in Balb/c mice. At day 5 p.i., the right lung lobes
382 of inoculated mice were collected, fixed, processed, and (A) stained with hematoxylin and eosin. Mock-infected
383 mice showed no significant pathology (Table S4). Scale bars indicate 200 μm (top panels) or 20 μm (lower
384 panels). (B, C) The severity of the pathology in individual lungs was assessed in a blind manner, and an overall
385 score out of 4 for the various categories of damage was assigned (infil; infiltrate, inf; inflammation, ly;
386 lymphocyte). Red bars indicate the median.

387

388 Conversely, the A28C Eng195 mutant gave lower average scores in all categories than its
389 WT counterpart and an overall highly significant difference of $p < 0.005$ (Fig 7C and Table
390 S4), confirming that mutation of the uAUG codon substantially attenuated virus

391 pathogenicity.



392
393
394
395
396
397
398
399

Figure 8. Pathogenesis of eNP-expressing viruses in CD-1 mice. Groups of 4-5 animals were infected with 10^4 PFU of PR8 viruses or 5×10^5 PFU of SW210 viruses. (A) Body weight was measured daily for up to 11 days. Animals that met the humane end-point were euthanized earlier. Data are the mean \pm SEM. ** $p < 0.01$, **** $p < 0.0001$ (t -tests between pairs of viruses). (B) For the SW210 pair of viruses, an additional six animals were included, and three animals were euthanized on each of days 3 and 5 p.i. for virus titres in lung homogenates to be determined. $p < 0.05$ (t -test between pairs of viruses on separate days).

400

401

BALB/c mice are biased towards Th2-type responses (32) and mouse strain-

402

dependent variations in response to pdm2009 infection have been observed (33).

403

Accordingly, to further test the effect of modulating NP start codons on viral pathogenicity,

404

we examined the course of infection in the outbred CD-1 mouse strain after infection with a

405

further two pairs of recombinant viruses differing only in the presence or absence of the

406

segment 5 uAUG codon: a complete clone of the SW210 pdm2009 virus, and the St Jude

407

Children's Hospital clone of PR8 (34). Infection with both WT and C28A mutant PR8

408

viruses led to severe weight loss from day 3 post infection onwards, resulting in all animals

409

reaching a humane endpoint by day 11. However, consistent with the previous experiment,

410

animals infected with the eNP-expressing mutant version of PR8 lost weight faster and died

411

sooner (Fig 8A). Infection with WT SW210 virus led to animals losing around 10% of their

412

body weight by day 7 followed by recovery from day 10. In contrast, the A28C derivative did

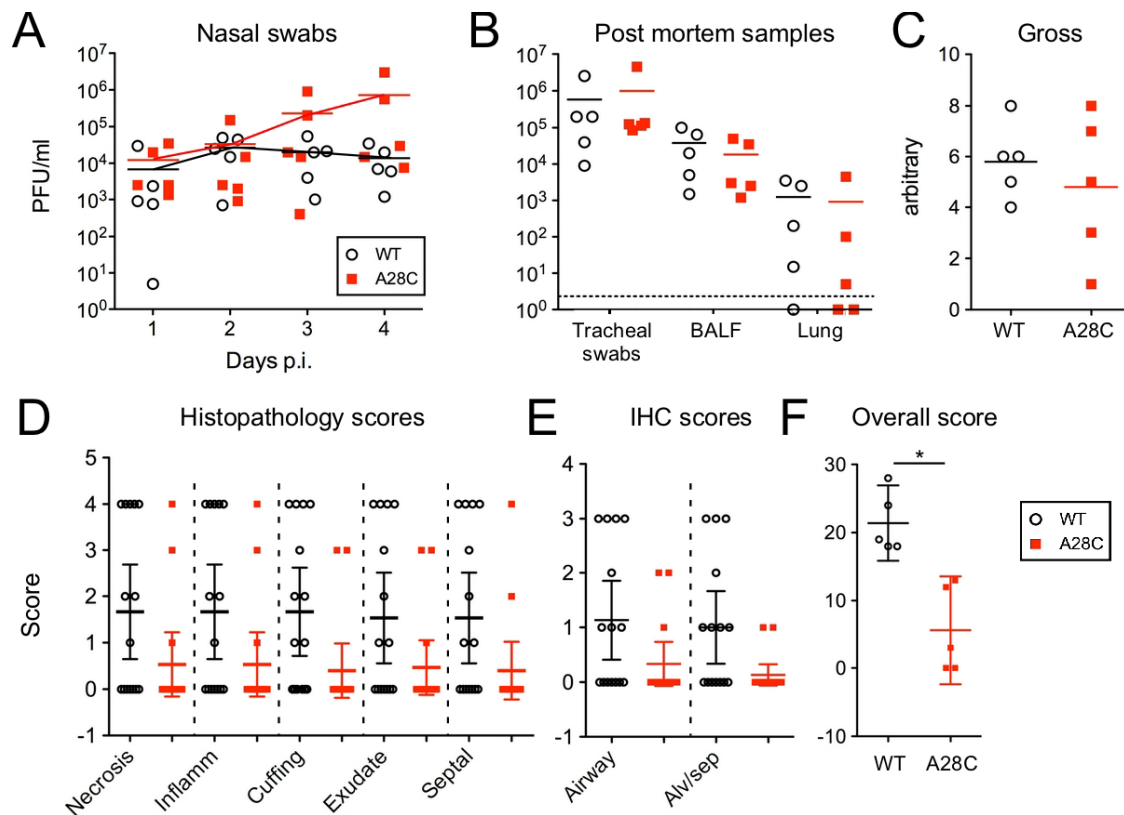
413

not cause any evident disease (Fig 8A). Examination of lung titres taken at days 3 and 5 p.i.

414

confirmed that the animals were infected but that the WT SW210 virus had replicated to titres

415 over 1 log₁₀ higher than the A28C mutant (Fig 8B), indicating that removal of the NP uAUG
 416 codon was attenuating *in vivo* in the background of an authentic pdm2009 virus. Thus, the
 417 attenuating effect of altering the uAUG codon was consistent across virus strains and breeds
 418 of mice.
 419



420
 421 **Figure 9.** Pathogenesis of a pdm2009 virus with altered eNP expression in pigs. Inbred Babraham pigs were
 422 challenged with WT or A28C Eng194 and (A, B) swabs and samples taken as indicated and titred for
 423 virus. Dashed line indicates the limit of detection. (C) Following necropsy at day 4 p.i., lungs were
 424 removed and scored for gross pathology. (D, E) Cut tissue sections were blinded and (D), stained with
 425 H&E and scored for the indicated categories of pathology or (E), stained for NP and scored for the
 426 quantity of viral antigen-positive cells. (F) – Iowa overall score, taking D and E together. * = p < 0.05
 427 (Mann Whitney *t*-test).

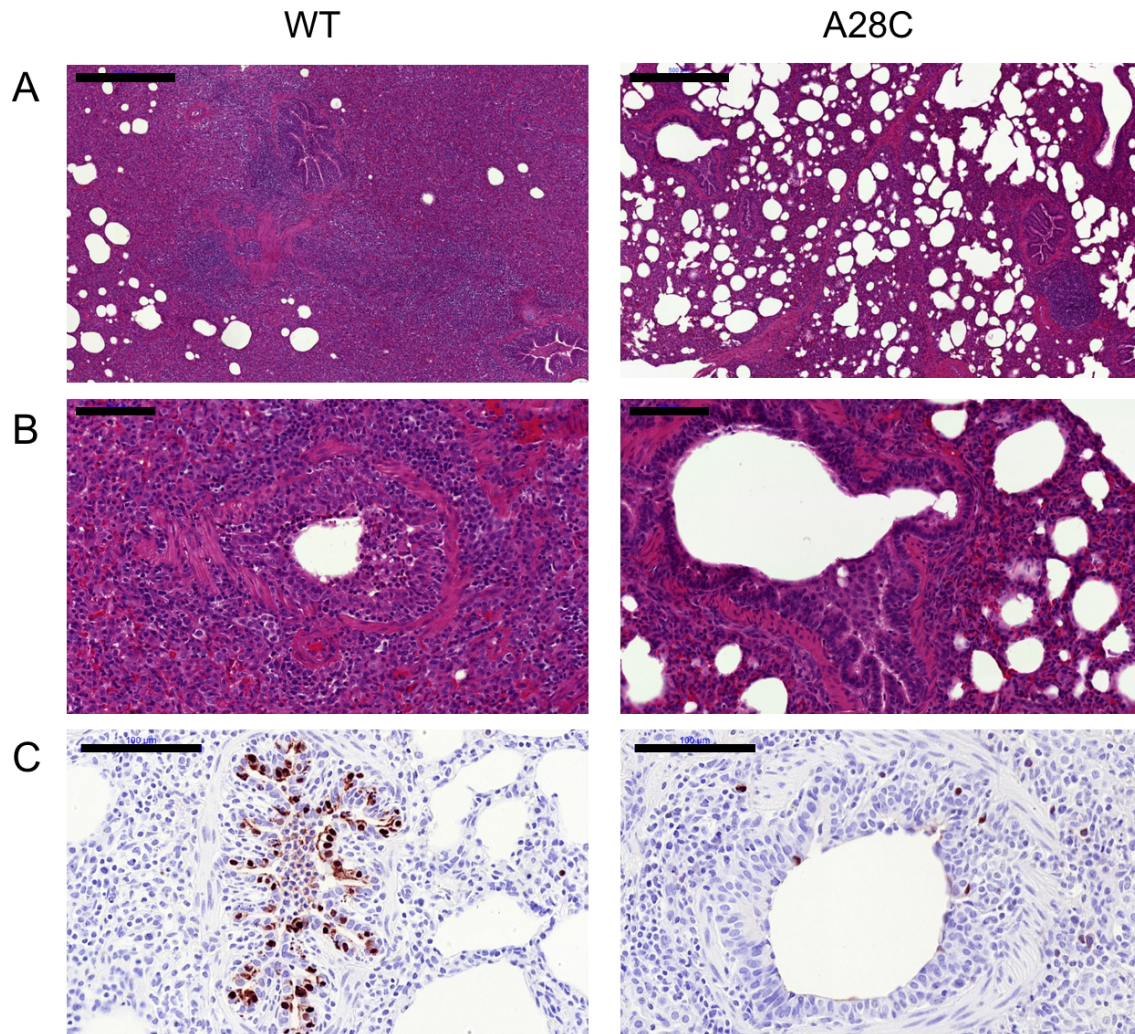
428

429

430 **The C28A polymorphism influences pathogenesis in pigs**

431 With evidence from the mouse model of IAV infection that the presence of the
432 segment 5 uAUG increased virulence, we tested whether this phenotype was replicated in
433 pigs, where uAUG appeared to be strongly selected for in an evolutionary context. For this,
434 we utilised a previously characterised challenge system using Babraham inbred pigs (35-37)
435 for the Eng195 virus. Groups of animals were infected intranasally with 2.2×10^5 PFU of WT
436 or A28C Eng195 and monitored for virus shedding by daily nasal swabs for 4 days. All
437 animals shed detectable levels of virus for the duration of the experiment and although the
438 average titres were higher from animals infected with the A28C virus at days 3 and 4 p.i. (Fig
439 9A), the data were variable and the differences were not statistically significant. At day 4 p.i.,
440 animals were euthanized and samples taken from the respiratory tract for virus titration.
441 Titres were highest in tracheal swabs, intermediate in bronchiolar lavage fluid (BALF) and
442 lowest in lung tissue homogenates, where not all samples were detectably positive (Fig 9B).
443 As with the shedding data, there were no significant differences between the two viruses
444 however. Examination of the animals' lungs showed areas of interstitial pneumonia and
445 atelectasis mostly in the apical lung lobes (Fig S7). However, the overall macroscopic
446 pathology scores between the two groups were also not significantly different (Fig 9C). To
447 examine microscopic pathology, five tissue samples per right lung (two apical and one each
448 from the medial, diaphragmatic and accessory lobes) were formalin fixed, processed into
449 paraffin-wax and cut sections stained with H&E. Histopathological analysis showed
450 multifocal interstitial pneumonia, attenuation/necrosis of bronchial and bronchiolar epithelial
451 cells, presence of inflammatory cell infiltrates within the interalveolar septa and the alveolar
452 lumen, and oedema (Fig 10A, B). These histopathological changes were scored across all
453 sections by a board-certified veterinary pathologist according to five parameters: necrosis of
454 the bronchiolar epithelium, airway inflammation, perivascular/bronchiolar cuffing, alveolar
455 exudates, and septal inflammation. Here, a clear difference between the two viruses became

456 apparent, with the A28C virus on average provoking lesser amounts of damage to the lung by
457 each criterion (Fig 9D). To assess virus spread within the lung, sections were stained by IHC
458 for IAV NP. Viral NP was observed mainly within the bronchial and bronchiolar epithelial
459 cells (Figure 10C), but also within inflammatory cells infiltrating into the bronchiolar



460

461 **Figure 10.** Histopathological analyses of pig lungs 4 days post challenge with WT and A28C Eng195 viruses.
462 Representative sections of lung stained with (A, B) H&E and imaged at low (scale bar = 500 μm) and high
463 (scale bar = 100 μm) magnification respectively or (C) stained for IAV NP (in brown) and counterstained with
464 haematoxylin. Scale bar = 100 μm .

465

466 lumen and alveolar spaces. NP-IHC staining was scored for the numbers of antigen-positive
467 cells in airway epithelia and alveolar septa/lumens, showing reduced numbers of cells

468 infected with the A28C mutant (Fig 9E). When histopathological and IHC scores were
469 combined to provide an overall measure of pathology (the “Iowa” scale) (35), animals
470 infected with the WT virus had consistent and significantly worse disease than those infected
471 with the A28C mutant virus (Fig 9F). Thus, removing the uAUG codon from a pdm2009
472 virus led to reduced virulence in a biologically relevant large animal model of IAV infection.
473

474 **Discussion**

475 The pdm2009 virus possesses several genetic features which might have explained its
476 unexpectedly mild disease characteristics in humans, including an avian IAV-like signature at
477 PB2 residue 627 and truncated PB1-F2, PA-X and NS1 genes. However, artificially altering
478 these sequences to what could reasonably be predicted to be a more pathogenic form and
479 testing them in animal models of infection has generally failed to support a causative role in
480 disease attenuation (6,36-42). Here, we investigated another genetic quirk of the pdm2009
481 virus; the presence of an extra in-frame start codon in the 5’-UTR of the NP gene. We found
482 that this uAUG originally emerged in classical swine viruses circulating in the early 1960s,
483 before being inherited by various reassortant lineages of viruses including the pdm2009
484 strain. We showed that the uAUG codon is used for translation initiation to produce two
485 isoforms of NP in infected cells, in a roughly 3:1 ratio of “normal” and “extended” [eNP]
486 polypeptides. This had little apparent functional consequence *in vitro*, either for viral gene
487 expression (something that NP plays a crucial role in) or for overall virus replication.
488 However, while the presence or absence of the uAUG did affect pathogenicity in mice and in
489 pigs, it acted to increase rather than decrease virulence in both animal models of infection.
490 Importantly, this included pigs, where the human pandemic strain originated. Thus, once
491 again, investigation of an unusual genetic feature of the pdm2009 virus has not supported the
492 simple hypothesis of an attenuating role in virulence.

493 A previous study has examined the functional significance of the segment 5 uAUG;
494 the authors did not directly determine whether it was actually used for translation initiation,
495 but using RNP reconstitution assays, they concluded that its presence significantly influenced
496 viral transcriptional activity, albeit only by around 2-fold (7). Here, we saw similar
497 magnitude effects, but without achieving statistical significance (Fig 2). We consider such
498 small fluctuations in minireplicon activity unlikely to have much biological consequence;
499 viruses with the same mutations replicated similarly in a variety of *in vitro* settings and had
500 no obvious deficits in gene expression (Fig 3). The question therefore remains, of how the
501 presence of the uAUG might enhance virulence. Whilst it is difficult to rule out subtle effects
502 arising directly from the UTR mutation (*e.g.* on segment 5 RNA synthesis or packaging),
503 these were normal as far as we could measure (Figs 4, 5). Instead, we prefer the hypothesis
504 that the *in vivo* phenotypic change results from the expression of a new isoform of NP. The
505 question then arises of how the function of the novel polypeptide varies from that of NP.

506 The N-terminal 20 amino acids of the canonical form of NP appear to be flexible, as
507 they are not visible in crystal structures of the whole protein (11,12,43). The primary function
508 attributed to this region of NP is that of a non-classical nuclear localization signal (ncNLS)
509 that binds cellular importin α (14,44-46). It is therefore possible that the addition of the 6
510 amino acids unique to the eNP sequence could affect interactions with importin α ; the much
511 larger (50 amino acid) extension on the related influenza B virus NP has been shown to affect
512 nuclear localization of the protein (47). However, the structure of the IAV NP ncNLS bound
513 to importin α suggests that this would not necessarily be the case here, as it binds to the
514 relatively shallow minor NLS-binding site, leaving the N-terminus of the NP sequence free,
515 where a short extension could easily be accommodated (46). In addition, we did not see any
516 appreciable differences in NP intracellular trafficking arising from the presence or absence of
517 eNP during a time course of infection in A549 cells (data not shown). The N-terminal

518 disordered region of NP is also a target for regulatory post-translational modification, such as
519 phosphorylation (48-50) and sumoylation (51); again something that could potentially be
520 affected by the addition of the 6 amino acids unique to eNP. However, the post translational
521 modifications only occur on a small fraction of the NP molecules in the cell and would
522 presumably still occur normally on canonical NP, which remains the most abundant isoform
523 in cells infected with a virus containing the uAUG codon. Thus, any changes to post
524 translational modification of eNP seem unlikely to be the primary cause of the phenotypic
525 effects seen here.

526 Our working hypothesis is therefore that acquisition of the segment 5 uAUG codon
527 represents a gain-of-function mutation for porcine IAV, reflecting a novel function for eNP
528 versus NP. Since NP has not been convincingly associated with any intrinsic enzymatic
529 activity, this would most simply be explained by the additional sequence mediating a new (or
530 stronger) interaction with a cellular binding partner that affects the outcome of *in vivo*
531 infection, but without affecting virus replication *in vitro*, at least in the cell lines tested. At
532 present, we do not have candidates for such a cellular factor and further experimentation is
533 required to identify these. Another question that remains to be answered is whether eNP
534 modulates pathogenesis through incorporation into viral RNPs, or as an isolated protein.

535 We found through evolutionary analyses that the segment 5 uAUG is primarily a trait
536 associated with virus strains of swine origin, where its recurrent emergence and fixation in
537 the major swine virus lineage implies it provides a host-specific selective advantage. This
538 hypothesis is consistent with the reduced virulence exhibited by pdm2009 virus engineered to
539 lack the uAUG codon (Figs 9, 10). Whether the uAUG codon provides a selective advantage
540 in the human host is also unclear, but the sporadic emergence of the uAUG in humans prior
541 to 2009 without provoking a selective sweep implies these events, and its dissemination in

542 2009, were driven by founder effect. However, its subsequent maintenance in the human
543 pdm2009 lineage (Table S2) gives no sign that it is being selected against in humans.

544 In summary, we have characterised a swine host-specific mutation in the 5'UTR of
545 IAV segment 5 which introduces an alternative start codon in frame with the NP ORF that
546 adds 6 amino acids to the N-terminus of the protein. This mutation modulates virulence in
547 mice and pigs, and was introduced to the human population via the 2009 pandemic. This
548 knowledge adds to our ability to understand and predict IAV virulence in specific hosts and
549 furthermore, suggests that the tendency for IAV sequencing efforts to disregard the viral
550 UTRs may be missing useful information.

551

552 **Materials and Methods**

553 *Bioinformatics*

554 On 31 Jan 2019, all full-length NP nucleotide sequences of IAV (any host, any location, any
555 year) were downloaded from Genbank via the NCBI Influenza Virus Resource database. The
556 sequences were named using the schema:

557 “>{serotype}_{host}_{accession}_{strain}_{country}_{year}/{month}/{day}_{segname}”.

558 50471 sequences in total were downloaded and of these there were 48288 with known
559 subtype, host, country and year. These were screened for duplicates and quality (number of
560 ambiguities), leaving 48245 good quality sequences which were padded with 10 codons (30
561 nucleotides) and then roughly aligned for further processing. However, although these
562 sequences were tagged as ‘full length’, not all of them reported sequence before the usual NP
563 start codon, leaving 33622 which had 5'UTR data suitable for analysis, representing 69.7%
564 of the good quality sequences. In order to determine in which major lineages the sequences
565 with upstream start codons occur, a stratified subsampling was performed, based on a
566 maximum of 1 sample per joint category of host + subtype + country or state (if USA,

567 Canada, China or Russia) + year + upstream start codon. This type of subsampling retains
568 the diversity of hosts, subtypes, locations, dates and start codons but will skew the
569 percentages of hosts vs start codons. The subsampling resulted in a data set of 6242
570 sequences, which were aligned using MUSCLE in MEGA and manually adjusted (at the far
571 3' end of the coding region which was not guaranteed to be complete by the process).

572 To construct phylogenetic trees, phylogeny was calculated from the stratified subsample
573 of 6242 sequences using RAxML with the GTR model allowing for a gamma distribution of
574 variable site rates and 100 bootstraps. Detailed time-resolved phylogenetic trees of selected
575 lineages or clades of the 6242 sequences dataset were inferred with BEAST (1.10.4) (52)
576 using the SRD06 codon partitioned nucleotide model with uncorrelated relaxed log normal
577 clock models and the constant population size or skygrid tree priors. Per lineage or clade,
578 1000 trees were sampled from the resulting posterior distribution of trees (after 10% burn-in).
579 For each selected clade or lineage, the start codon was mapped as a binary variable
580 (Conventional or Upstream) onto the set of 1000 posterior trees using a discrete trait
581 asymmetric model in BEAST, resulting in a set of 10,000 trees (approximately 10 mappings
582 per original tree), which were summarised to a maximum clade credibility tree using
583 TreeAnnotator

584

585 *Plasmids and antisera.*

586 Each of the eight IAV segments used throughout were encoded on IAV reverse gene
587 plasmids containing bi-directional RNA polymerase I and II promoters. Two different PR8
588 strains were used: most experiments used an MDCK-adapted variant of the UK National
589 Institute of Biological Standards and Control vaccine strain of PR8 (53), while data shown in
590 figure 7 used an egg-adapted PR8 strain described previously (28,34). Plasmids for the
591 A/England/195/2009 (Eng/195; an early UK pdm09 strain) are described in (22), while those

592 for A/Halifax/210/2009 (SW210; an early pandemic isolate from the Queen Elizabeth II
593 Hospital, Halifax, Nova Scotia, Canada) are described in (54). A plasmid encoding a gene
594 fusion between the 5'-201 nucleotides of PR8 segment 5 and GFP was made by PCR-cloning
595 the appropriate IAV sequence into pEGFP-1 (Clontech), followed by oligonucleotide-
596 directed PCR mutagenesis (using standard protocols) to remove the A of the GFP AUG
597 codon. Nucleotide substitutions in the segment 5 plasmids to modify AUG motifs were made
598 by further rounds of oligonucleotide-directed mutagenesis. To create the 4c6c PR8 virus with
599 a genome packaging defect, codons 546-548 of the PR8 HA gene were synonymously
600 mutated to **tTaGGtGCc** and codons 451 to 453 of PR8 NA were mutated to **tcaATaGAt**
601 (altered nucleotides indicated in lower case bold, all sequences given in (+) sense). Primer
602 sequences are available on request. Sequence modifications to plasmids were confirmed by
603 commercial Sanger sequencing (GATC, Eurofins Genomics) before being used in
604 downstream experiments.

605 For western blotting, purchased antisera used were: mouse monoclonal anti-GFP
606 (clone JL8, Clontech), rat monoclonal anti- β tubulin (clone YL1/2, Abd-Serotech) and mouse
607 monoclonal anti-IAV NP (clone AA5H, Abd-Serotech). In-house rabbit polyclonal antisera
608 raised against IAV PB1, PB2, NP and M1 have been previously described (55-57).
609 Secondary antibodies labelled with infrared-fluorescent dyes were obtained from Fisher. For
610 IHC staining of cut tissue sections, mouse monoclonal anti-NP (hybridoma HB-65 from
611 ATCC (Manassas, VA, USA)) was used.

612

613 *Viruses.*

614 Virus rescues were performed as previously described (27,58). Briefly, 293T cells
615 were transfected with 250ng each of the 8 plasmids from a viral reverse genetics set (or no
616 segment 5 as a negative control), with 1 μ g/ml tosyl phenylalanyl chloromethyl ketone

617 (TPCK)-treated trypsin added at 48 hours post-transfection. At 72-96 hours post-transfection,
618 supernatants were harvested and either passaged on MDCK cells in serum free medium with
619 1µg/ml TPCK-treated trypsin, or 100 µl was inoculated into the allantoic cavity of 12 day-old
620 embryonated hen's eggs, the allantoic fluid of which was harvested at day 14 and aliquoted
621 as virus stock. Titres were determined by plaque assay on MDCK (PR8; at 37°C) or MDCK-
622 SIAT cells (59)(Eng/195; at 35°C). Plaques on MDCK cells were typically visualized by
623 toluidine blue staining, while plaques on MDCK-SIAT cells were immunostained for viral
624 NP. The presence of the desired mutations in the virus genome was confirmed by RT-PCR
625 and Sanger sequencing of RNA isolated from the virus stocks. Early-passage H1N1 pdm2009
626 clinical isolates A/Nottingham/Adult-Community04/2009 (AC04), A/Nottingham/Child-
627 Community06/2009 (CC06) and A/Nottingham/Child-Community07/2009 (CC07) were
628 isolated and passaged twice on MDCK cells as described (29,64).

629

630 *Cells and transfection methods*

631 293T, MDCK, A549, and NPTr cells were grown in DMEM supplemented with 10%
632 FBS and 1% penicillin and streptomycin (Fisher) and maintained by twice weekly passage.
633 IAV minireplicon assays were performed as described (27). Briefly, unless otherwise stated,
634 50ng each of pDUAL plasmids encoding segment 1,2, 3 and 5 and 20ng of a construct that
635 expresses an IAV-like vRNA encoding luciferase were transfected into 293T cells in 24 well
636 format. Transfected cells were harvested in 100 µl cell culture lysis reagent (Promega) and 60
637 µl supernatants were mixed with 25 µl 6mM beetle luciferin (Promega). Luminescence was
638 measured on a GloMax luminometer (Promega). Assays were performed using four technical
639 replicates for each datapoint as well as at least three biological repeats.

640

641 *Protein methods*

642 *In vitro* translation reactions were performed using coupled bacteriophage T7 RNA
643 polymerase transcription-rabbit reticulocyte lysate translation reactions as per the
644 manufacturer's instructions (Promega TNT). Samples were radiolabelled with ³⁵S-methionine
645 (Perkin Elmer) and detected by SDS-PAGE and autoradiography. To separate eNP and NP,
646 samples were loaded onto 10% pre-cast gels (BioRad) and run until the 50kDa ladder marker
647 had just run off the bottom of the gel. For western blotting, wet transfers were performed,
648 membranes were blocked with 5% milk for 30-60 minutes then incubated with specific
649 antibodies in 2% BSA at 4°C overnight. The next day, membranes were incubated with
650 secondary anti-rabbit or anti-mouse IgG antibodies conjugated to fluorophore AlexaFluor
651 680 or 800 as required, before imaging using a LiCor Odyssey FC.

652 To purify virus, allantoic fluid was clarified twice by centrifugation for 10 min at
653 2100 x g, then loaded onto a 30% sucrose/PBS cushion and spun at 30,000 rpm using an
654 SW28Ti Beckman rotor for 1 hour and 30 min at 4°C. The resulting pellet was gently washed
655 once with 500 µl of PBS to remove residual sucrose and re-suspended back in 50 µl of PBS
656 overnight. The virus was further purified by ultracentrifugation through a 15-60% sucrose
657 gradient (in PBS) spun at 38,000rpm for 40 min using a Beckman SA41Ti rotor at 4°C. The
658 virus band was extracted from the gradient using a syringe and virus pelleted by
659 centrifugation at 30,000 rpm for 90 min at 4°C before being resuspended as above.

660 For cytokine arrays of mouse lung homogenates, 20 µl of lung homogenate per mouse
661 was collected and pooled within groups. Cytokines were then measured using Proteome
662 Profiler Mouse Cytokine Array Kit (R&D Biosystems) according to manufacturer's
663 instructions. Arrays were imaged and spot intensities quantified using a LI-COR Odyssey
664 Infrared Imaging System (LI-COR, Cambridge, UK). Following normalization to within-
665 assay control spots values were plotted as fold increase in cytokine expression over mock-
666 infected animals.

667

668 *Ethics statement.*

669 Animal experimentation was approved by the Roslin Institute Animal Welfare and Ethical
670 Review Board, the Pirbright Institute Ethical Review Board under the authority of Home
671 Office project licences (60/4479 and 70/7505 respectively) within the terms and conditions of
672 the UK Home Office “Animals (Scientific Procedures) Act 1986“ and associated guidelines,
673 or in compliance with the guidelines of the Canadian Council on Animal Care (CCAC) as
674 outlined in the Care and Use of Experimental Animals, Vol. 1, 2nd Edn. (1993). In this case,
675 the animal care protocol was approved by the University of Ottawa Animal Care Committee
676 (Protocol Number: BMI-85) and all efforts were made to minimize suffering and mice were
677 euthanized at humane end-points, if infection resulted in greater than 30% body weight loss
678 plus respiratory distress.

679

680 *Mouse infections.*

681 BALB/c mice were purchased from Harlan UK Ltd (Oxon, UK), CD-1 mice were purchased
682 from Charles River Laboratories, (Montreal, Quebec, Canada). Five- to 12-week-old female
683 mice were used in all experiments. Mice were anaesthetized using isoflurane (Merial Animal
684 Health Ltd) and infected intranasally with virus in 40 µl serum-free DMEM. Mice were
685 weighed daily and assessed for visual signs of clinical disease, including inactivity, ruffled
686 fur and laboured breathing. At day 5-post infection, mice were euthanized by CO₂
687 asphyxiation. Virus titration and RNA extraction and qRT-PCR was undertaken as
688 previously described (60). Briefly, left lung homogenates were collected in 500 µl DMEM
689 and homogenised using a Qiagen TissueLyser II. For virus titration, standard plaque assays
690 on MDCK cells were performed and the remaining supernatant was used for RNA
691 quantification. RNA was extracted using a Qiagen Viral RNA mini kit according to

692 manufacturer's instructions and DNase treated using Promega RQ1-RNase free DNase.
693 RT-qPCR was undertaken using a BioLine Sensifast one step RT-qPCR kit with modified
694 cycling conditions of 45°C for 10 minutes, 95°C for 2 minutes, then 40 cycles of 95°C for
695 10s and 60°C for 30s. Primer sequences are given in Table 2. For histopathological analysis,
696

697 **Table 2.** Sequences of primers used for RT-qPCR.
698

Gene	Polarity	Sequence
Seg2	Sense	GGAACAGGATACACCATGGA
	Antisense	AGTGGYCCATCAATCGGGTT
Seg 5	Sense	ATCATGGCGTCTCAAGGCAC
	Antisense	CCGACGGATGCTCTGATTTC
GAPDH	Sense	CTACCCCAATGTGTCCGTCG
	Antisense	GATGCCTGCTTACCACCTTC
IFN- β	Sense	CACAGCCCTCTCCATCAACT
	Antisense	GCATCTTCTCCGTCATCTCC

699
700 the four lobes of the right lung were inflated with and then immersed in 10% neutral buffered
701 formalin (Sigma-Aldrich) until fixed, then processed using routine methods and embedded in
702 paraffin blocks. 5 μ m thin section were then cut and stained with haematoxylin and eosin for
703 histological examination. Sections were assessed (blinded) by a veterinary pathologist
704 (PMB). The individual pathology features assessed were damage to the airway epithelium
705 (degeneration, necrosis and repair), perivascular inflammation, peribronchi/bronchiolar
706 inflammation, interstitial inflammation, interstitial necrosis and type II pneumocyte
707 hyperplasia. Each feature was scored from 1 (mild) to 3 (marked). The percentage of lung
708 affected was also noted.

709

710 *Pig infection model*

711 Ten 12-14 wk old Babraham large white inbred pigs (average weight 30 kg) were obtained
712 from the Pirbright Institute/ Animal Plant Health Agency. Pigs were screened for absence of

713 influenza infection by hemagglutination inhibition using four swine IAV antigens. Pigs were
714 randomly divided into two groups. and were inoculated intranasally with 2.2×10^5 PFU virus.
715 Two milliliters were administered to each nostril using a MAD300 mucosal atomization
716 device (Wolfe Tory Medical). Four nasal swabs (two per nostril) were taken daily after the
717 challenge. Two nasal swabs were placed in 2 ml virus transport medium for the quantification
718 of viral load by plaque assay as previously described (61). The other two nasal swab samples
719 were put directly into TRIzol (Invitrogen, ThermoFisher Scientific, UK) for subsequent RNA
720 isolation according to the manufacturer's instructions. Animals were humanely killed 5 d
721 post challenge. At post mortem, the lungs were removed, and photographs taken of the dorsal
722 and ventral aspects. Macroscopic pathology was scored blind, as previously reported (62).
723 Tracheal swabs, bronchoalveolar lavage and the accessory lobe were collected to determine
724 the viral load in the lower respiratory tract by plaque assay. In brief, the accessory lobe was
725 cut into small pieces and homogenised with a gentleMACS Octo Dissociator (Miltenyi
726 Biotec) using C tubes (Miltenyi Biotec) in ice cold Dulbecco's PBS supplemented with 0.1%
727 BSA. The lung homogenates (10% w/v) were centrifuged and the clarified supernatant was
728 used to determine the viral load and for RNA isolation. The tracheal swabs were processed
729 like the nasal swabs. BALF was collected as previously described (61) and cell-free
730 supernatant used to determine viral load. For histopathology, five lung tissue samples per
731 animal from the right lung (two pieces from the apical, one from the medial, one from the
732 diaphragmatic and one from the accessory lobe) were collected into 10% neutral buffered
733 formalin for routine histological processing at the University of Surrey. Formalin-fixed
734 tissues were paraffin wax-embedded, and 4 μm sections were cut and stained with H&E.
735 Immunohistochemical staining of IAV NP was performed in 4 μm tissue sections as
736 previously described (63). Histopathological changes in the stained lung tissue sections were
737 scored by a veterinary pathologist blinded to the treatment group. Lung histopathology was

738 scored using five parameters (necrosis of the bronchiolar epithelium, airway inflammation,
739 perivascular/bronchiolar cuffing, alveolar exudates and septal inflammation) scored on a five-
740 point scale of 0 to 4 and then summed to give a total slide score ranging from 0 to 20 and a
741 total animal score from 0 to 100 (64). The Iowa system includes both histological lesions and
742 immunohistochemical staining for NP (35). Sequencing of segment 5 from virus-positive
743 samples from pigs confirmed that viruses produced during infection encoded uAUG or not,
744 as expected (data not shown).

745

746 **Acknowledgements**

747 We thank Dr Ben Killingley for clinical virus isolates, Dr Ed Hutchinson for critical
748 comments, the Easter Bush Pathology Service staff for assistance and the animal staff at the
749 Roslin and Pirbright Institutes and University of Ottawa for animal care.

750

751 **Disclosures**

752 JSN-V-T is currently seconded to the Department of Health and Social Care (DHSC),
753 England. The views expressed in this manuscript are those of the authors and not necessarily
754 those of DHSC.

755

756 **Funding information**

757

758 This work was funded by Institute Strategic Programme Grants (BB/J01446X/1 and
759 BB/P013740/1) from the UK Biotechnology and Biological Sciences Research Council
760 (BBSRC) to PD, BMD, PMB, EG and SJL, as well as BBS/E/I/00007030 and
761 BBS/E/I/00007031 to ET and PMB, a National Institute for Health Research (Grant: 09/85
762 FLU-DRP) to JSN-V-T, a Canadian Institutes of Health Research (CIHR) Pandemic

763 Preparedness Team grant (no. TPA-90188) to the CIHR Canadian Influenza Pathogenesis
764 Team (EGB) and a CIHR Institute of Infection and Immunity (<http://www.cihr-irsc.gc.ca/>)
765 operating grant (MOP-74526) to EGB. EG is supported by a Wellcome Trust/ Royal Society
766 Sir Henry Dale Fellowship (211222/Z/18/Z), while SJL is supported by a University of
767 Edinburgh Chancellor's Fellowship. KK was supported by a Wellcome Trust PhD
768 studentship (no. 086157).
769

770 Bibliography

- 771 1. Dawood FS, Iuliano AD, Reed C, Meltzer MI, Shay DK, Cheng PY, et al. Estimated
772 global mortality associated with the first 12 months of 2009 pandemic influenza A
773 H1N1 virus circulation: A modelling study. *Lancet Infect Dis.* 2012 Sep 1;12(9):687–
774 95.
- 775 2. Simonsen L, Spreeuwenberg P, Lustig R, Taylor RJ, Fleming DM, Kroneman M, et al.
776 Global Mortality Estimates for the 2009 Influenza Pandemic from the GLaMOR
777 Project: A Modeling Study. Hay SI, editor. *PLoS Med.* Public Library of Science;
778 2013 Nov 1;10(11):e1001558.
- 779 3. Garten RJ, Garten RJ, Davis CT, Davis CT, Russell CA, Russell CA, et al. Antigenic
780 and genetic characteristics of swine-origin 2009 A(H1N1) influenza viruses circulating
781 in humans. *Science.* 2009 Jul 10;325(5937):197–201.
- 782 4. Jagger BW, Jagger BW, Wise HM, Wise HM, Kash JC, Kash JC, et al. An
783 overlapping protein-coding region in influenza A virus segment 3 modulates the host
784 response. *Science.* 2012 Jul 13;337(6091):199–204.
- 785 5. Shi M, Shi M, Jagger BW, Jagger BW, Wise HM, Wise HM, et al. Evolutionary
786 conservation of the PA-X open reading frame in segment 3 of influenza A virus. *J*
787 *Virol.* 2012 Nov;86(22):12411–3.
- 788 6. Hale BG, Steel J, Medina RA, Manicassamy B, Ye J, Hickman D, et al. Inefficient
789 control of host gene expression by the 2009 pandemic H1N1 influenza A virus NS1
790 protein. *J Virol.* American Society for Microbiology; 2010 Jul;84(14):6909–22.
- 791 7. Wanitchang A, Wanitchang A, Patarasirin P, Patarasirin P, Jengarn J, Jengarn J, et al.
792 Atypical characteristics of nucleoprotein of pandemic influenza virus H1N1 and their
793 roles in reassortment restriction. *Arch Virol.* 2011 Jun;156(6):1031–40.
- 794 8. Portela A, Portela A, Digard P. The influenza virus nucleoprotein: a multifunctional
795 RNA-binding protein pivotal to virus replication. *J Gen Virol.* 2002 Apr;83(Pt 4):723–
796 34.
- 797 9. Einfeld AJ, Neumann G, Kawaoka Y. At the centre: influenza A virus
798 ribonucleoproteins. *Nat Rev Microbiol.* 2015 Jan;13(1):28–41.
- 799 10. Kukol A, Hughes DJ. Large-scale analysis of influenza A virus nucleoprotein
800 sequence conservation reveals potential drug-target sites. *Virology.* 2014 Apr 1;454-
801 455:40–7.
- 802 11. Ye Q, Krug RM, Tao YJ. The mechanism by which influenza A virus nucleoprotein
803 forms oligomers and binds RNA. *Nature.* 2006 Dec 21;444(7122):1078–82.
- 804 12. Ng AK-L, Ketha KMV, Atreya CD, Zhang H, Tan K, Li Z, et al. Structure of the
805 influenza virus A H5N1 nucleoprotein: implications for RNA binding,
806 oligomerization, and vaccine design. *BMC Cell Biol.* 2008;9(10):22–3647.
- 807 13. O'Neill RE, Palese P. NPI-1, the human homolog of SRP-1, interacts with influenza
808 virus nucleoprotein. 1995 Jan 10;206(1):116–25.

- 809 14. Neumann G, Neumann G, Castrucci MR, Castrucci MR, Kawaoka Y, Kawaoka Y.
810 Nuclear import and export of influenza virus nucleoprotein. *J Virol.* 1997
811 Dec;71(12):9690–700.
- 812 15. Wu WW, Sun Y-HB, Panté N. Nuclear import of influenza A viral ribonucleoprotein
813 complexes is mediated by two nuclear localization sequences on viral nucleoprotein.
814 *Virology*. BioMed Central Ltd; 2007 Jun 4;4(1):49.
- 815 16. Taubenberger JK, Kash JC. Influenza virus evolution, host adaptation, and pandemic
816 formation. *Cell Host Microbe.* 2010 Jun 25;7(6):440–51.
- 817 17. Wang R, Taubenberger JK. Characterization of the noncoding regions of the 1918
818 influenza A H1N1 virus. *J Virol.* American Society for Microbiology Journals; 2014
819 Feb;88(3):1815–8.
- 820 18. Pulit-Penaloza JA, Belser JA, Tumpey TM, Maines TR. Sowing the Seeds of a
821 Pandemic? Mammalian Pathogenicity and Transmissibility of H1 Variant Influenza
822 Viruses from the Swine Reservoir. *Trop Med Infect Dis.* Multidisciplinary Digital
823 Publishing Institute; 2019 Feb 27;4(1):41.
- 824 19. Zhu Q, Yang H, Chen W, Cao W, Zhong G, Jiao P, et al. A naturally occurring
825 deletion in its NS gene contributes to the attenuation of an H5N1 swine influenza virus
826 in chickens. *J Virol.* 2008 Jan;82(1):220–8.
- 827 20. Kozak M. Point mutations define a sequence flanking the AUG initiator codon that
828 modulates translation by eukaryotic ribosomes. *Cell.* 1986 Jan 31;44(2):283–92.
- 829 21. Wise HM, Wise HM, Barbezange C, Jagger BW, Dalton RM, Gog JR, et al.
830 Overlapping signals for translational regulation and packaging of influenza A virus
831 segment 2. *Nucleic Acids Research.* 2011 Sep 1;39(17):7775–90.
- 832 22. Brookes DW, Miah S, Lackenby A, Hartgroves L, Barclay WS. Pandemic H1N1 2009
833 influenza virus with the H275Y oseltamivir resistance neuraminidase mutation shows
834 a small compromise in enzyme activity and viral fitness. *J Antimicrob Chemother.*
835 2011 Mar;66(3):466–70.
- 836 23. Diaz de Arce AJ, Noderer WL, Wang CL. Complete motif analysis of sequence
837 requirements for translation initiation at non-AUG start codons. *Nucleic Acids*
838 *Research.* 2018 Jan 25;46(2):985–94.
- 839 24. Peabody DS. Translation initiation at non-AUG triplets in mammalian cells. *J Biol*
840 *Chem.* 1989 Mar 25;264(9):5031–5.
- 841 25. Dasso MC, Jackson RJ. On the fidelity of mRNA translation in the nuclease-treated
842 rabbit reticulocyte lysate system. *Nucleic Acids Res.* Oxford University Press; 1989
843 Apr 25;17(8):3129–44.
- 844 26. Huang TS, Palese P, Krystal M. Determination of influenza virus proteins required for
845 genome replication. *Journal of Virology.* American Society for Microbiology (ASM);
846 1990 Nov;64(11):5669–73.

- 847 27. Wise HM, Foeglein Á, Sun J, Dalton RM, Patel S, Howard W, et al. A complicated
848 message: Identification of a novel PB1-related protein translated from influenza A
849 virus segment 2 mRNA. *J Virol.* 2009 Aug;83(16):8021–31.
- 850 28. Lin L, Li Y, Pyo H-M, Lu X, Raman SNT, Liu Q, et al. Identification of RNA helicase
851 A as a cellular factor that interacts with influenza A virus NS1 protein and its role in
852 the virus life cycle. *J Virol.* 5 ed. American Society for Microbiology Journals; 2012
853 Feb;86(4):1942–54.
- 854 29. Killingley B, Greatorex J, Digard P, Wise H, Garcia F, Varsani H, et al. The
855 environmental deposition of influenza virus from patients infected with influenza
856 A(H1N1)pdm09: Implications for infection prevention and control. *Journal of*
857 *Infection and Public Health.* King Saud Bin Abdulaziz University for Health Sciences;
858 2015 Dec 1;:1–11.
- 859 30. Kirchbach von JC, Gog JR, Digard P. Genome packaging in influenza A virus. *J Gen*
860 *Virol.* 2010 Feb;91(Pt 2):313–28.
- 861 31. Gog JR, Afonso EDS, Dalton RM, Leclercq I, Tiley L, Elton D, et al. Codon
862 conservation in the influenza A virus genome defines RNA packaging signals. *Nucleic*
863 *Acids Research.* Oxford University Press; 2007;35(6):1897–907.
- 864 32. Mills CD, Kincaid K, Alt JM, Heilman MJ, Hill AM. M-1/M-2 macrophages and the
865 Th1/Th2 paradigm. *J Immunol.* 2000 Jun 15;164(12):6166–73.
- 866 33. Otte A, Gabriel G. 2009 pandemic H1N1 influenza A virus strains display differential
867 pathogenicity in C57BL/6J but not BALB/c mice. *Virulence.* 2011 Nov;2(6):563–6.
- 868 34. Hoffmann E, Krauss S, Perez D, Webby R, Webster RG. Eight-plasmid system for
869 rapid generation of influenza virus vaccines. *Vaccine.* 2002 Aug 19;20(25-26):3165–
870 70.
- 871 35. Gauger PC, Vincent AL, Loving CL, Henningson JN, Lager KM, Janke BH, et al.
872 Kinetics of lung lesion development and pro-inflammatory cytokine response in pigs
873 with vaccine-associated enhanced respiratory disease induced by challenge with
874 pandemic (2009) A/H1N1 influenza virus. *Vet Pathol.* 2012 Nov;49(6):900–12.
- 875 36. Zhu H, Wang J, Wang P, Song W, Zheng Z, Chen R, et al. Substitution of lysine at
876 627 position in PB2 protein does not change virulence of the 2009 pandemic H1N1
877 virus in mice. *Virology.* 2010 May 25;401(1):1–5.
- 878 37. Pena L, Vincent AL, Loving CL, Henningson JN, Lager KM, Lorusso A, et al.
879 Restored PB1-F2 in the 2009 pandemic H1N1 influenza virus has minimal effects in
880 swine. *J Virol.* American Society for Microbiology; 2012 May;86(10):5523–32.
- 881 38. Hai R, Schmolke M, Varga ZT, Manicassamy B, Wang TT, Belser JA, et al. PB1-F2
882 expression by the 2009 pandemic H1N1 influenza virus has minimal impact on
883 virulence in animal models. *J Virol.* 2010 May;84(9):4442–50.
- 884 39. Gao H, Sun Y, Hu J, Qi L, Wang J, Xiong X, et al. The contribution of PA-X to the
885 virulence of pandemic 2009 H1N1 and highly pathogenic H5N1 avian influenza
886 viruses. *Sci Rep.* Nature Publishing Group; 2015 Feb 5;5(1):8262.

- 887 40. Lee J, Yu H, Li Y, Ma J, Lang Y, Duff M, et al. Impacts of different expressions of
888 PA-X protein on 2009 pandemic H1N1 virus replication, pathogenicity and host
889 immune responses. *Virology*. 2017 Apr;504:25–35.
- 890 41. Jagger BW, Memoli MJ, Sheng Z-M, Qi L, Hrabal RJ, Allen GL, et al. The PB2-
891 E627K mutation attenuates viruses containing the 2009 H1N1 influenza pandemic
892 polymerase. 2010 Apr;1(1).
- 893 42. Tu J, Guo J, Zhang A, Zhang W, Zhao Z, Zhou H, et al. Effects of the C-terminal
894 truncation in NS1 protein of the 2009 pandemic H1N1 influenza virus on host gene
895 expression. Pekosz A, editor. *PLoS ONE*. Public Library of Science;
896 2011;6(10):e26175.
- 897 43. Chenavas S, Estrozi LF, Slama-Schwok A, Delmas B, Di Primo C, Baudin F, et al.
898 Monomeric nucleoprotein of influenza A virus. 2013 Mar 1;9(3):e1003275.
- 899 44. Wang P, Palese P, O'Neill RE. The NPI-1/NPI-3 (karyopherin alpha) binding site on
900 the influenza A virus nucleoprotein NP is a nonconventional nuclear localization
901 signal. *J Virol*. 1997 Mar;71(3):1850–6.
- 902 45. Cros JF, García-Sastre A, Palese P. An unconventional NLS is critical for the nuclear
903 import of the influenza A virus nucleoprotein and ribonucleoprotein. *Traffic*.
904 Blackwell Publishing Ltd; 2005 Mar;6(3):205–13.
- 905 46. Nakada R, Hirano H, Matsuura Y. Structure of importin- α bound to a non-classical
906 nuclear localization signal of the influenza A virus nucleoprotein. *Sci Rep*. Nature
907 Publishing Group; 2015 Oct 12;5:15055.
- 908 47. Sherry L, Smith M, Davidson S, Jackson D. The N terminus of the influenza B virus
909 nucleoprotein is essential for virus viability, nuclear localization, and optimal
910 transcription and replication of the viral genome. García-Sastre A, editor. *J Virol*. 5 ed.
911 American Society for Microbiology Journals; 2014 Nov;88(21):12326–38.
- 912 48. Arrese M, Portela A. Serine 3 is critical for phosphorylation at the N-terminal end of
913 the nucleoprotein of influenza virus A/Victoria/3/75. *Journal of Virology*. American
914 Society for Microbiology (ASM); 1996 Jun;70(6):3385–91.
- 915 49. Hutchinson EC, Denham EM, Thomas B, Trudgian DC, Hester SS, Ridlova G, et al.
916 Mapping the phosphoproteome of influenza A and B viruses by mass spectrometry.
917 Gack MU, editor. *PLoS Pathog*. Public Library of Science; 2012;8(11):e1002993.
- 918 50. Zheng W, Li J, Wang S, Cao S, Jiang J, Chen C, et al. Phosphorylation Controls the
919 Nuclear-Cytoplasmic Shuttling of Influenza A Virus Nucleoprotein. Lyles DS, editor.
920 *Journal of Virology*. American Society for Microbiology Journals; 2015 Jun
921 1;89(11):5822–34.
- 922 51. Han Q, Chang C, Li L, Klenk C, Cheng J, Chen Y, et al. Sumoylation of influenza A
923 virus nucleoprotein is essential for intracellular trafficking and virus growth. *J Virol*.
924 American Society for Microbiology; 2014 Aug;88(16):9379–90.
- 925 52. Drummond AJ, Rambaut A. BEAST: Bayesian evolutionary analysis by sampling
926 trees. *BMC evolutionary biology*. BioMed Central; 2007 Nov 8;7(1):214.

- 927 53. de Wit E, Spronken MIJ, Bestebroer TM, Rimmelzwaan GF, Osterhaus ADME,
928 Fouchier RAM. Efficient generation and growth of influenza virus A/PR/8/34 from
929 eight cDNA fragments. *Virus Res.* 2004 Jul;103(1-2):155–61.
- 930 54. Park H-S, Liu G, Thulasi Raman SN, Landreth SL, Liu Q, Zhou Y. NS1 Protein of
931 2009 Pandemic Influenza A Virus Inhibits Porcine NLRP3 Inflammasome-Mediated
932 Interleukin-1 Beta Production by Suppressing ASC Ubiquitination. López S, editor. *J*
933 *Virol.* American Society for Microbiology Journals; 2018 Apr 15;92(8):55.
- 934 55. Carrasco M, Amorim MJ, Digard P. Lipid raft-dependent targeting of the influenza A
935 virus nucleoprotein to the apical plasma membrane. *Traffic.* 2004 Dec;5(12):979–92.
- 936 56. Noton SL, Medcalf E, Fisher D, Mullin AE, Elton D, Digard P. Identification of the
937 domains of the influenza A virus M1 matrix protein required for NP binding,
938 oligomerization and incorporation into virions. *J Gen Virol.* 2007 Aug;88(Pt 8):2280–
939 90.
- 940 57. Amorim MJ, Read EK, Dalton RM, Medcalf L, Digard P. Nuclear export of influenza
941 A virus mRNAs requires ongoing RNA polymerase II activity. *Traffic.* 2007
942 Jan;8(1):1–11.
- 943 58. Hutchinson EC, Curran MD, Read EK, Gog JR, Digard P. Mutational analysis of cis-
944 acting RNA signals in segment 7 of influenza A virus. *J Virol.* 2008
945 Dec;82(23):11869–79.
- 946 59. Matrosovich M, Matrosovich T, Carr J, Roberts NA, Klenk H-D. Overexpression of
947 the alpha-2,6-sialyltransferase in MDCK cells increases influenza virus sensitivity to
948 neuraminidase inhibitors. *Journal of Virology.* American Society for Microbiology
949 Journals; 2003 Aug;77(15):8418–25.
- 950 60. Gaunt E, Wise HM, Zhang H, Lee LN, Atkinson NJ, Nicol MQ, et al. Elevation of
951 CpG frequencies in influenza A genome attenuates pathogenicity but enhances host
952 response to infection. *Elife.* eLife Sciences Publications Limited; 2016;5:e12735.
- 953 61. Morgan SB, Holzer B, Hemmink JD, Salguero FJ, Schwartz JC, Agatic G, et al.
954 Therapeutic Administration of Broadly Neutralizing FI6 Antibody Reveals Lack of
955 Interaction Between Human IgG1 and Pig Fc Receptors. *Front Immunol.* Frontiers;
956 2018;9:865.
- 957 62. Halbur PG, Paul PS, Frey ML, Landgraf J, Eernisse K, Meng XJ, et al. Comparison of
958 the pathogenicity of two US porcine reproductive and respiratory syndrome virus
959 isolates with that of the Lelystad virus. *Vet Pathol.* 1995 Nov;32(6):648–60.
- 960 63. Vidaña B, Martínez J, Martínez-Orellana P, García Migura L, Montoya M, Martorell J,
961 et al. Heterogeneous pathological outcomes after experimental pH1N1 influenza
962 infection in ferrets correlate with viral replication and host immune responses in the
963 lung. *Vet Res.* BioMed Central; 2014;45(1):85.
- 964 64. Morgan SB, Hemmink JD, Porter E, Harley R, Shelton H, Aramouni M, et al. Aerosol
965 Delivery of a Candidate Universal Influenza Vaccine Reduces Viral Load in Pigs
966 Challenged with Pandemic H1N1 Virus. *J Immunol.* American Association of
967 Immunologists; 2016 Jun 15;196(12):5014–23.

968

969 **Supplementary Information**

970

971 **Table S1.** Distribution of NP start codons by major IAV lineage in the stratified subsampled
972 data set.

Host-lineage	Avian	Swine	Human	Other	Total Sequences	Conventional Start %	uAUG Start %
Avian-Americas	2642	2	2	5	2651	99.9	0.1
Avian-Eurasia	1449	22	56	46	1573	99.6	0.4
Equine-Canine	0	2	0	71	73	100.0	0.0
Human-pdm2009	2	6	232	0	240	2.1	97.9
Human-Seasonal	1	28	894	1	924	99.6	0.4
Swine-Classical-Triple	15	352	23	0	390	8.7	91.3
Swine-Eurasia	1	68	4	0	73	94.5	5.5
Variant-pdm2009	2	122	181	4	309	7.8	92.2
Unclassified	2	1	0	6	9	100.0	0.0

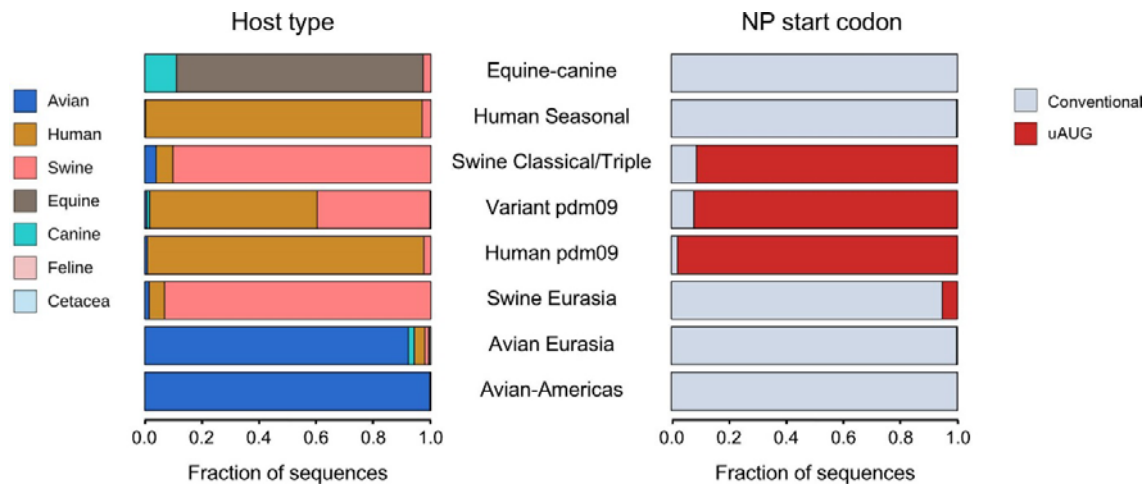
973

974 In the stratified subsampled data set of 6242 segment 5 sequences, the distribution of NP start
975 codons by host was similar to that in the full data set, although the percentage of
976 sequences with an upstream start codon was somewhat reduced compared to the full
977 data set (see Table 1).

978 **Table S2. (see separate Excel file).** Stratified subsampled dataset of IAV segment 5
979 sequences, classified according to the presence (TRUE) or absence (FALSE) of an in-
980 frame upstream AUG codon in the NP gene, as well as H and N subtype, continent,
981 region and country of isolation, host and date of isolation and named clade. The
982 position of the first AUG codon in the segment (first_start) and the identity of the
983 nucleotide triplet at the location of the uAUG (upstream3) are also tabulated.

984

985

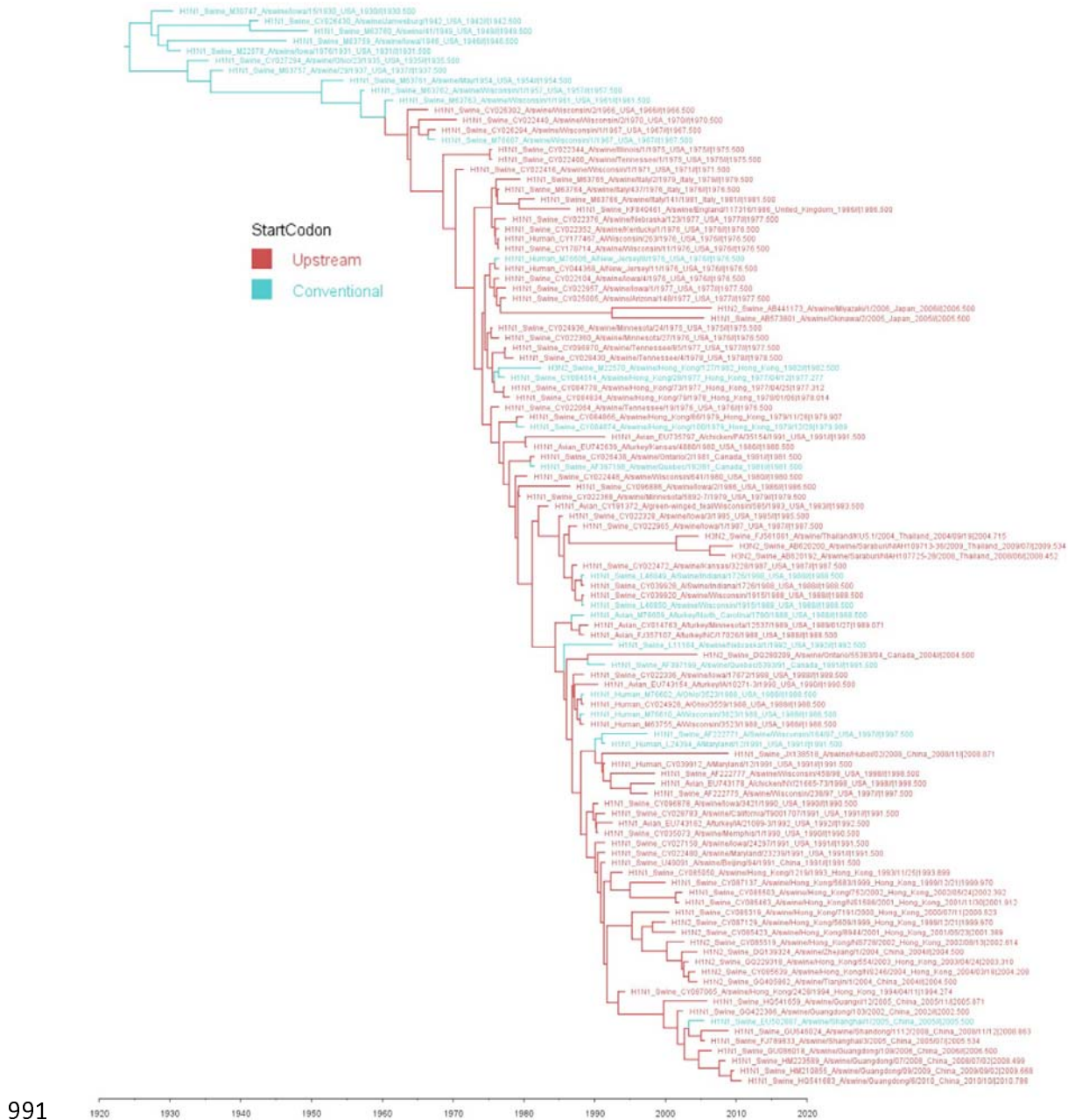


986

987 **Figure S1.** Distribution of hosts and segment 5 start codon positions by major IAV lineage in
988 the stratified subsampled data set.

989

990



991

992 **Figure S2.** Time scaled tree of segment 5 from the classical swine virus clade with skygrid
 993 tree prior and NP start codon as a discrete trait. Sequences in red possess the uAUG,
 994 those in blue do not. The uAUG codon first appeared at an estimated date in 1962
 995 (range 1958-1965) in H1N1 swine IAV in Wisconsin. This is based on the mutation
 996 happening somewhere on the branch between nodes 1960.41 [Highest Posterior
 997 Density (HPD): 1958.1 - 1961.5] and 1963.55 [HPD: 1961.2 - 1965.7]).

998

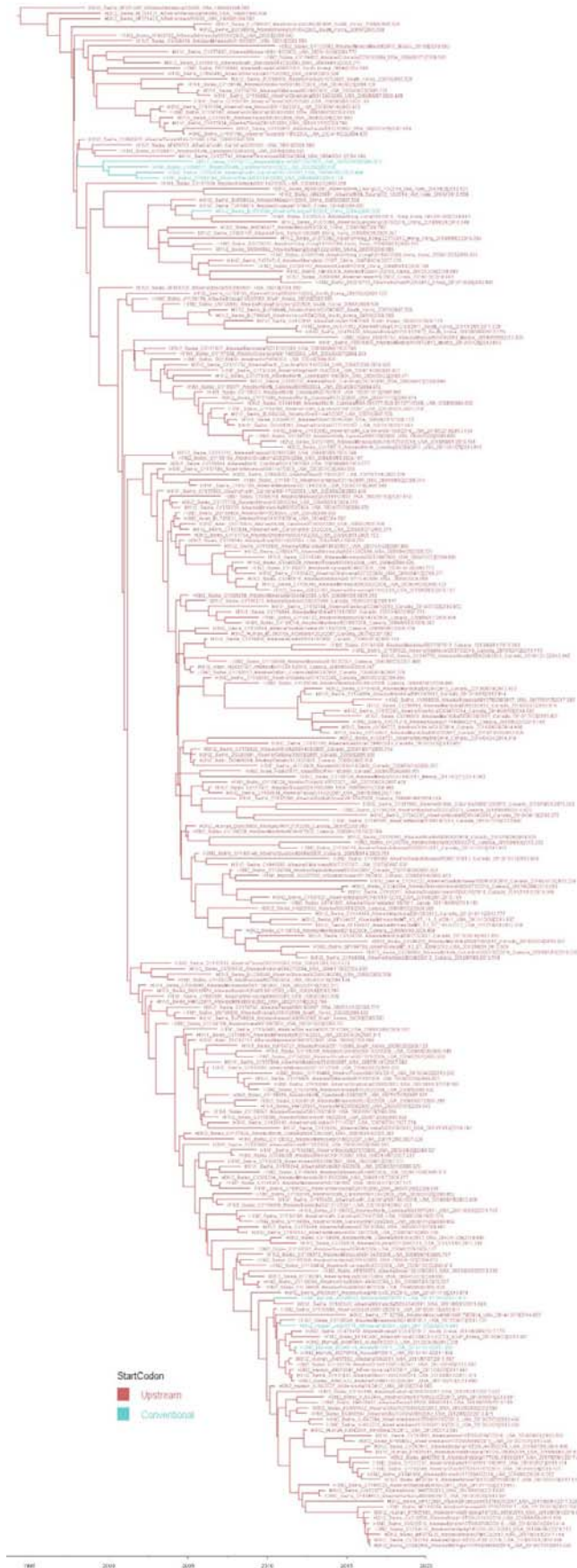


Figure S3. Time scaled tree of segment 5 from the triple reassortant swine virus clade with skygrid tree prior and NP start codon as a discrete trait. Sequences in red possess the uAUG, those in blue do not. Triple reassortant viruses most likely inherited an uAUG-containing segment 5 from their classical swine progenitor and subsequently, have largely kept it.

Strain	Accession	Host	Subtype	Country
A/duck/New_York/16873/1999	CY014891	Avian	H6N2	USA
A/mallard/Maryland/887/2002	EU026010	Avian	H6N1	USA
A/chicken/Italy/322/2001	CY021552	Avian	H7N1	Italy
A/chicken/Israel/702/2008	GQ148843	Avian	H9N2	Israel
A/duck/Taiwan/DC167/2010	KC693624	Avian	H1N3	Taiwan
A/Albany/20/1974	CY021096	Human	H3N2	USA
A/Bilthoven/2271/1976	KC296468	Human	H3N2	Netherlands
A/Singapore/64K/2007	KP223188	Human	H3N2	Singapore
A/Victoria/600/2016	CY254980	Human	H3N2	Australia

1024

1025 **Table S3.** Sporadic occurrences of the uAUG in avian and human seasonal viruses. Isolate
1026 name, subtype, segment 5 sequence accession code, host and country of isolation are
1027 tabulated. Most isolates are too temporally and/or geographically separate to represent
1028 linked events; the H6 duck isolates from the eastern USA in 1999 and 2002 and the
1029 human H3N2 isolates from the mid 1970s might be exceptions.

1030

1031

1032

1033



1034

1035 **Figure S4.** Acquisition of the segment 5 uAUG codon associated with epizootic transfer
1036 from ducks to swine. A time scaled tree of segment 5 from an avian virus clade with skygrid
1037 tree prior and NP start codon as a discrete trait. Sequences in red possess the uAUG, those in
1038 blue do not. The 5'-UTR sequence of segment 5 from the closest relative of the uAUG-
1039 possessing A/swine/Fujian/2001 and /2003 viruses (A/duck/Zhejiang/11/2000(H5N1)) has
1040 not been reported, making it uncertain whether the polymorphism occurred before or after the
1041 host-range jump. Note also that the apparent persistence of the uAUG-containing swine virus
1042 in China until 2014 may be an artefact, as all eight segments of A/swine/Shandong/SD1/2014
1043 have the corresponding genes from A/swine/Fujian viruses from the early 2000s as their
1044 closest relatives (> 99.7% nucleotide identity) and conversely, lack close relatives from the
1045 2010s, raising the possibility of laboratory contamination.
1046

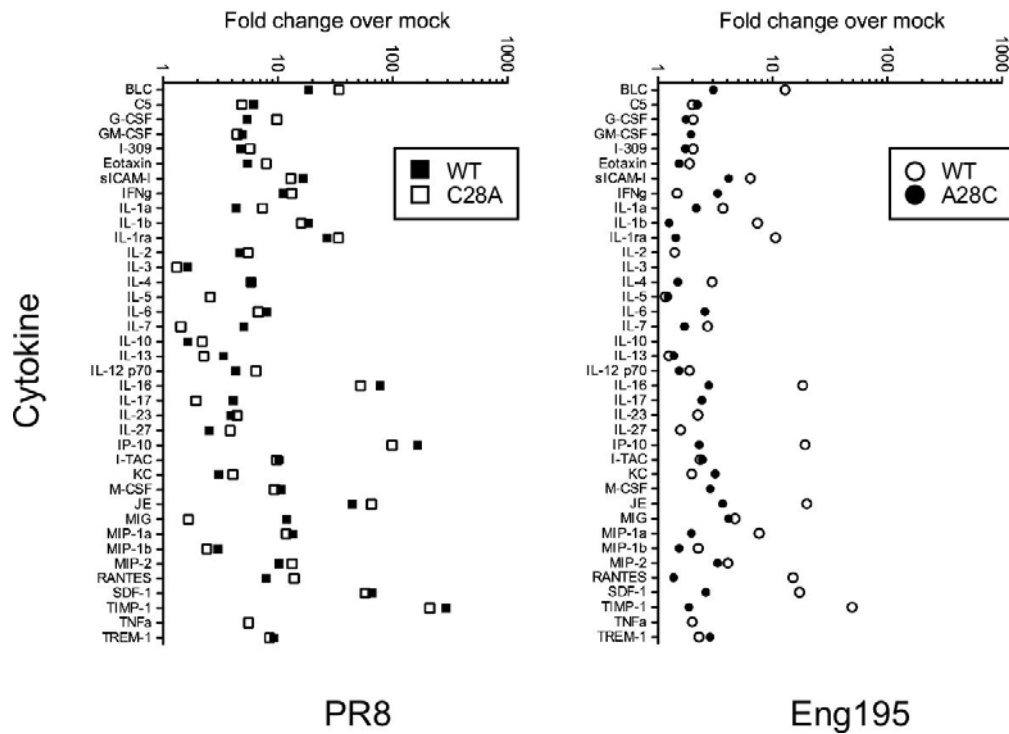


1047
1048
1049
1050
1051
1052

Figure S5. Acquisition of the segment 5 uAUG codon within the Eurasian swine IAV lineage. A time scaled tree of segment 5 from an avian virus clade with skygrid tree prior and NP start codon as a discrete trait. Sequences in red possess the uAUG, those in blue do not.

1053

1054



1055

1056

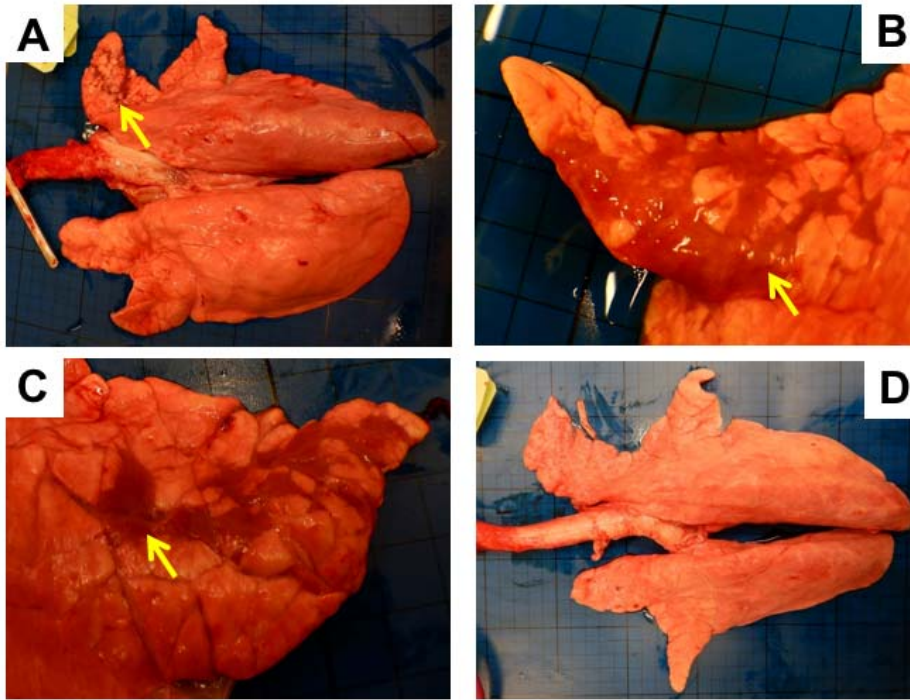
1057 **Figure S6.** Cytokine levels in infected mouse lung. Lung homogenates from mice infected
1058 with the indicated viruses or mock infected animals were pooled and the levels of
1059 various cytokines measured by cytokine array.

1060

1061 **Table S4.** (see separate Excel file). Formalin-fixed lung sections were stained with
1062 haematoxylin and eosin and examined by a veterinary pathologist. Six pathological changes
1063 (epithelial cell degeneration and necrosis, perivascular inflammation, peribronchial
1064 inflammation, interstitial inflammation, interstitial necrosis and lymphocyte cuffing) were
1065 scored on a scale of 0-4. The percentage of lung affected was estimated visually. The
1066 pathological changes present along with a consideration of the area of lung affected was used
1067 to give an overall qualitative score of the severity of histopathological changes. Slides from
1068 three mice (22, 14 and 9) were not scored and excluded from the analysis due to marked
1069 atelectasis (artefact) which precluded assessment of pathological changes.

1070

1071
1072
1073



1074
1075
1076
1077
1078
1079
1080

Figure S7. Macroscopic pathology of pig lungs 4 days post challenge with WT (A, B and C) and A28C Eng195 (D) viruses. Arrows indicate areas of atelectasis observed in the apical lobe of the right lung (A) and medial lobes (B and C). Some animals from the A28C group exhibited no remarkable gross pathology (D).